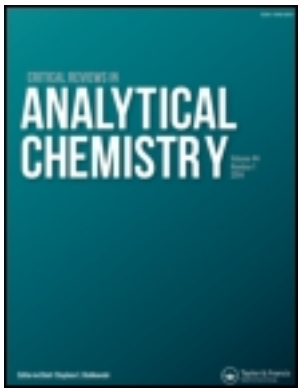

Critical Reviews in Analytical Chemistry
Publication details, including instructions for authors and subscription information:
http://www.tandfonline.com/loi/batc20

Progress in Thermal Lens Spectrometry and Its Applications in Microscale Analytical Devices

Mingqiang Liu[a] & Mladen Franko[a]
[a] Laboratory for Environmental Research, University of Nova Gorica, Nova Gorica, Slovenia
Published online: 15 May 2014.

To cite this article: Mingqiang Liu & Mladen Franko (2014) Progress in Thermal Lens Spectrometry and Its Applications in Microscale Analytical Devices, Critical Reviews in Analytical Chemistry, 44:4, 328-353, DOI: 10.1080/10408347.2013.869171

To link to this article: http://dx.doi.org/10.1080/10408347.2013.869171

Critical Reviews in Analytical Chemistry, 44:328–353, 2014

ISSN: 1040-8347 print / 1547-6510 online
DOI: 10.1080/10408347.2013.869171

Progress in Thermal Lens Spectrometry and Its Applications in Microscale Analytical Devices

Mingqiang Liu and Mladen Franko
Laboratory for Environmental Research, University of Nova Gorica, Nova Gorica, Slovenia

Development of thermal lens spectrometry (TLS) as a micro space-compatible photothermal technique and its applications for analysis of different chemical compounds in micro space and particularly in microfluidic systems are reviewed. Theoretical treatment of TLS in micro space has evolved from simply following conventional theory and predictions in macro space to employing a more accurate theory where impacts of the excitation source (Gaussian laser, top-hat incoherent light source, beam divergence, power density), detection scheme (probe beam waist, mode-mismatching degree), sample flow, and sample cell (top/bottom layers, side wall) on the TL signal are included. Noise sources (light sources, sample status, detector) in TLS systems have been analyzed, and optimum pinhole-to-beam radius ratio is suggested for the maximum signal-to-noise ratio. With different excitation light sources from ultraviolet, to visible, to near-infrared regions and coupled with microfluidic devices, these TLS instruments with good temporal and spatial resolution have found many applications for highly sensitive and/or high-throughput detection of chemical or biochemical analytes, for cell imaging or single particle/molecule detection, and for characterization of molecular diffusion in single- or two-phase systems. Prospects and challenges of TLS for future applications in microchemical analysis are discussed.

Keywords Chemical/environmental applications, microfluidics, thermal lens spectrometry

INTRODUCTION

Research and development on downsizing and integration of chemical systems on a chip, namely "lab-on-a-chip," are now the trend in chemistry and chemical analysis (Livak-Dahl et al., 2011; Tian and Finhout, 2008). By integrating different analytical processes for sequential operations like sampling, sample pretreatment, separation, derivatization reactions, and analyte detection in a microfluidic device (Kikutani et al., 2005), a micro total analysis system (μ-TAS) can be assembled to realize automated and controllable manipulation or detection of chemicals with very low reagent consumption and short analysis time in comparison with conventional chemical analysis. Microchips with simple or sophisticated channel networks for a wide variety of applications are commercially available from different companies, such as Micronit, Dolomite, microLIQUID, Microflexis, and Institute of Microchemical Technology.

In microfluidic devices, highly sensitive detectors are required to detect analytes in a microchannel with dimensions on the scale of several tens of micrometers. Detection methods mainly used in microfluidics can be classified into three major types: optical methods, electrochemical methods, and mass spectrometric (MS) methods (Wu and Gu, 2011). Electrochemical methods are very sensitive and can be implemented in field-portable devices, but they are suitable only for electroactive analytes and are sensitive to variations of the experimental conditions (such as temperature, flow rate of the liquid, contamination) (Crevillén et al., 2007; Váradi et al., 1979). MS is highly sensitive and requires only a small quantity of sample. But on the other hand, MS needs ionization of analytes and is not suitable for nonvolatile compounds (Lazar et al., 2006). Among the optical methods, fluorescence-based detection, due to its high sensitivity and compatibility with micro space, has found wide application in microfluidic device–based chemical analysis of trace analytes or even detection of single molecules (Okabare and Soper, 2009). However, this method is limited to fluorescent samples or fluorophore-derivatized nonfluorescent analytes. The majority of biologically important chemicals, such as amino acids, nucleotides, proteins, and hormones, are natively nonfluorescent and need to be derivatized before detection, which can bring unexpected interferences to the analysis or cause changes of the analyte. In contrast to the luminescence-based methods, thermal lens spectrometry (TLS) (Fang and Swoford, 1983), as one of the

Address correspondence to Mladen Franko, Laboratory for Environmental Research, University of Nova Gorica, P.O. Box 301, SI-5000 Nova Gorica, Slovenia. E-mail: mladen.franko@ung.si

Color versions of one or more of the figures in the article can be found online at www.tandfonline.com/batc.

photothermal techniques, depends on nonradiative relaxation processes and conversion of the absorbed energy into heat. In principle, any substance absorbing the light can be detected by TLS, even fluorescent compounds unless the fluorescence quantum yield equals unity (no absorbed light is converted to heat). TLS provides as high sensitivity as spectrofluorimetric methods, which enable detection of absorbances down to 10^{-7} AU (absorbance units), and as a method of molecular absorption spectroscopy, can exploit all the features and advantages of conventional spectrophotometry and cover a much larger spectrum of substances than fluorescence methods.

Different theoretical descriptions of the TL effect under a variety of experimental conditions and the applications of TLS in different analytical fields have been reviewed extensively in several books and review articles (Bialkowski, 1996; Dovichi, 1987; Fang and Swoford, 1983; Franko, 2008; Franko and Tran, 1996; Gupta, 1988; Harris, 1986; Navas and Jiménez, 2003; Proskurnin and Kononets, 2004). Besides its high sensitivity, TLS is also capable of fast and small-volume detection, which makes it suitable for coupling to an optical microscope to construct the so-called thermal lens microscope (TLM) (Harada et al., 1993). To make a clear distinction between TLM and other TLS instruments, which are mainly used for detection in long path length samples but also for detection in micro space, the term TLM will be used only for cases where the focusing of pump and probe beams onto the sample is achieved by a single objective lens and the beam sizes in the sample are ~ 1 μm.

With good temporal ($\sim$ ms) and spatial ($\sim \mu$m) resolutions, TLM has been developed into a promising detector for microfluidic analysis. Due to lower occurrence of some interfering or hindering substances and an increase in the degree of completeness of the analytical reaction in micro space, TLM has better detection selectivity and/or sensitivity than the conventional apparatus for the same sample path length in macro space (Proskurnin and Kononets, 2004). As reviewed before (Dudkoa et al., 2012; Ghaleb and Georges, 2004; Kitamori et al., 2004; Tokeshi et al., 2003), different TLM instruments have found many applications in chemical, biochemical/biomedical, and environmental fields for analysis of different compounds, such as metal ions, antigens, amino acids, catecholamines, cytochrome c, pharmaceuticals, and pesticides. In recent years, some new variations of TLM have been developed for specific applications, such as circular dichroism TLM in the UV region (UV-CD-TLM) for chiral analysis on a microchip (Mawatari et al., 2008), polarization modulation TLM (PM-TLM) for imaging the orientation of nonspherical nanoparticles (Zhang et al., 2011), and differential interference contrast TLM (DIC-TLM) in a microchannel or extended nanochannel for background-free detection of nanoparticles (Shimizu et al., 2009, 2010, 2011). With the development of a more accurate TL theoretical model (Liu et al., 2012), the signal-generation mechanism in micro space was better understood (Liu and Franko, 2013), incorporation of an incoherent light source (ILS) into the TLM as the excitation source was demonstrated as feasible (Liu and Franko, 2012), rapid detection of environmental samples was realized (Liu and Franko, 2014b), and molecular diffusion in a two-phase system in the microchannel was investigated (Liu et al., 2013) as well.

This review aims to provide an overview of the recent progress in developing TLS (especially TLM) instruments and their applications in micro space (especially in microfluidic devices) for chemical analysis. First, a basic theoretical background on microfluidics and TLS is given. Then, we illustrate instrument development and some typical applications, which are followed by a table listing most of the applications of TLS instruments in microfluidic devices. Finally, conclusions are made and prospects of the TLS for future microfluidic chemical analysis are indicated.

THEORETICAL BACKGROUND

Downscaling of a chemical analysis system from macro- to microscale not only brings much smaller reagent/sample consumption and more precise and controllable manipulation of fluids in a continuously flowing stream or in a localized compartment, but also much shorter reaction or incubation time. In this section, basic theories of fluid and/or molecular dynamics in micro space are briefly given and then the TLS models in a flowing medium are introduced.

Microfluidic Chip

There are several characteristic features of micro space contributing to short analysis time, for example, short diffusion distance, high interface-to-volume ratio (specific interface area between solid/liquid or liquid/liquid phases), and small heat capacity. To control molecular transport in micro space, the molecular transportation time and the specific interface area must be considered. The molecular transportation time is given by (Sato et al., 2003; Tokeshi et al., 2001a)

$$t_m = L_m^2/D_m \tag{1}$$

where t_m, L_m, and D_m are the molecular transportation time, diffusion distance, and diffusion coefficient, respectively. The specific interface area, σ_m, can be expressed as

$$\sigma_m = S_m/V_m \propto 1/L_m \tag{2}$$

where S_m and V_m are the interface area and the volume. Figure 1 shows the dependences of the molecular transportation time and the specific interface area on the diffusion distance. When D_{m} is on the order of 10^{-5} cm^2/s, as for most molecules and ions, the transportation takes several hours to a day when L_{m} is 1 cm, while only several tens of seconds is needed when L_{m} is 100 μm.

Depending on the driving mode of the liquid through a microchannel, different flow profiles in the cross section of the

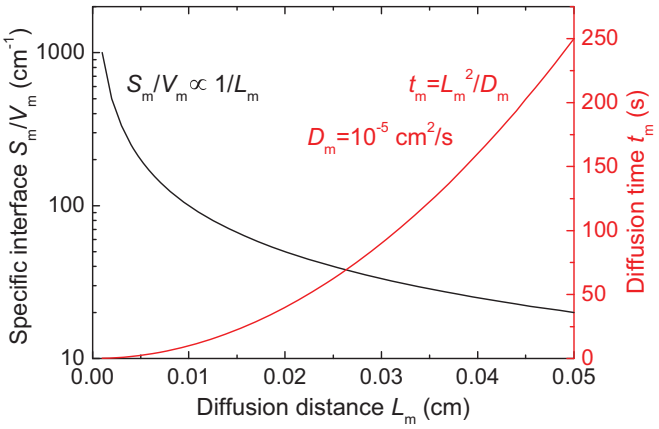

FIG. 1. Specific interface area and molecular transportation time as a function of the diffusion distance (from Sato et al., 2003a). © 2003 Elsevier B.V. Reproduced by permission of Elsevier B.V. Permission to reuse must be obtained from the rightsholder.

channel could appear. Two main flow types are electroosmotic flow, such as in capillary electrophoresis (CE), where the flow velocity in cross section is quasi-homogeneous, and laminar flow, when the liquid is driven by a microsyringe or pressure pump, for which the flow profile is parabolic. When there are two phases of fluids in a microchannel, a mathematical model including the convection and the diffusion terms should be employed to describe the molecular transfer between the two phases (Žnidaršič-Plazl and Plazl, 2007).

TLS in a Flowing Medium

In chemical analysis, especially in microfluidic devices, analytes are usually detected in flowing mediums. In Figure 2, schematic representations of collinear and crossed-beam TLS configurations in both transversal and coaxial flow modes are shown. Here, "collinear" and "crossed-beam" refer to the optical beam configurations of TLS, while "transversal" and "coaxial" express the azimuth between the flow direction of the liquid and the propagating direction of the pump beam. Obviously, configuration (d) is the best one from the point of view of absolute TL signal sensitivity and resistivity to effects of sample flow. However, for different sample cells or sample channel structures, such as a circular cell in micro space, other configurations have also found applications. The crossed-beam TLS configuration is normally used in those cases where the collinear configuration is difficult to realize or would bring higher noises, such as in CE, where configuration (a) is usually employed (Faubel et al., 2003). The transversal flow mode is employed only when the coaxial mode is not possible or inconvenient to perform, such as on a microchip, where configuration (b) was used (Kim et al., 2003), while in an 8 μL flowing cell, configuration (d) was implemented in a TLS system (Pogačnik and Franko, 2001).

For detection in TLS systems, it was already demonstrated that when the sample flows, the TL signal amplitude is reduced due to the displacement of TL outside the irradiated area. If the sample is flowing at a linear velocity sufficiently high to remove the heated element from the probe beam region on the time scale of the thermal time constant ($t_c = a_{e0}^2/(4D)$, with a_{e0} the pump beam waist radius and D the thermal diffusivity), the TL signal will be substantially decreased (Nickolaisen and Bialkowski, 1986; Weimer and Dovichi, 1985). This is more obvious in configurations (a) and (b) in Figure 2 than the latter two configurations of (c) and (d). It has been demonstrated for continuous-wave (CW) excitation that the highest sensitivity can be obtained by shifting the position of the probe beam along the direction of the flow (Vyas and Gupta, 1988; Weimer and Dovichi, 1985), while for the configurations (c) and (d), this is not necessary. The loss of sensitivity is much less pronounced in configuration (d). For example, in an 8 μL 1 cm path length cell, only 25% decrease in sensitivity was observed at 1 mL/min flow rate (Dovichi and Harris, 1981). This can be explained by more than one order of magnitude

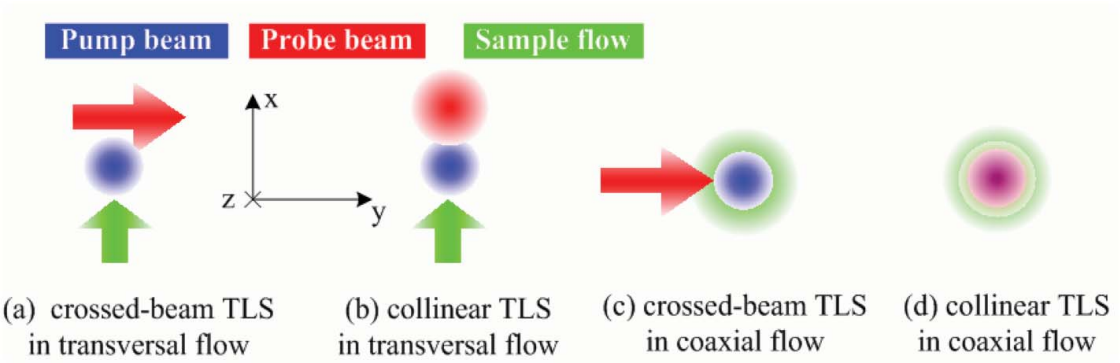

FIG. 2. Pump-probe beam configuration for crossed-beam ((a) and (c)) and collinear ((b) and (d)) TLS in transversal flow ((a) and (b)) and coaxial flow ((c) and (d)) modes in a flowing medium.

shorter TL time constants than the sample residence time. It should be noted that the decrease of TL signal by sample flow is also closely related to the modulation frequency of the pump beam under CW laser excitation or the pulse duration under pulsed laser excitation. In the case of pulsed excitation, because of very fast rise time (10 μs) of the maximal TL signal, very little variation (few percentages) in TL signal was observed for flow rates up to 10 mL/min even in the case of transversal flows (Chanlon and Georges, 2002; Nickolaisen and Bialkowski, 1986). Source noise limitations and subsequent poor precision are the main reasons why pulsed TLS is not used for detection in liquid chromatography (LC) and flow injection analysis (FIA), even though the sensitivity of the technique is not affected by the flow of the sample.

Besides the experimental works, theoretical models for TL signal in flowing medium have been developed (Liu et al., 2012; Vyas and Gupta, 1988). To obtain an explicit solution for the thermal diffusion equation, the flow of the sample was assumed homogeneous, with flow velocity v_x (Figure 3), which is half of the central flow velocity of the laminar flow. Under the parabolic approximation, the TL signal is expressed as

$$S(t) = \frac{z_1}{f_x(t)} + \frac{z_1}{f_y(t)} \tag{3}$$

where z_1 is the distance from the probe beam waist to the sample and $f_x(t)$ and $f_y(t)$ denote the focal lengths of the "ideal thin lens" in x- and y-directions, respectively. To improve the flow-induced sensitivity deterioration, the probe beam can be displaced with respect to the pump beam in the x-direction by a certain distance d, which is called pump-probe beam offset. For the collinear TL configuration, such as presented in Figure 3,

$$\frac{1}{f_x(t)} = -\frac{dn}{dT} l \left[\frac{\partial^2 T(x,y,t)}{\partial x^2}\right]_{\substack{x=d \\ y=0}},$$
$$\frac{1}{f_y(t)} = -\frac{dn}{dT} l \left[\frac{\partial^2 T(x,y,t)}{\partial y^2}\right]_{\substack{x=d \\ y=0}} \tag{4}$$

and for the crossed-beam TLS,

$$\frac{1}{f_x(t)} = -\frac{dn}{dT} \int_{-\infty}^{\infty} \left[\frac{\partial^2 T(x,y,t)}{\partial x^2}\right]_{x=d} dy,$$
$$\frac{1}{f_z(t)} = 0 \tag{5}$$

in which l denotes the effective sample length (or the thickness of the TL element), and dn/dT is the temperature coefficient of refractive index of the sample. Expressions for $T(x, y, t)$ under excitations of CW and pulsed lasers can be found in Vyas and Gupta (1988), and that under top-hat beam excitation can be found in Liu et al. (2012).

To more accurately describe the TL signal, the aberrant nature of the TL element should be accounted for, and in this case, the Fresnel diffraction theory, instead of the parabolic approximation, was employed. The complex electric field distribution of the probe beam in the detection plane is expressed as

$$E_2(x_2, y_2, d, z_1 + z_2, t) = \frac{j\exp(-jkz_2)}{2\lambda z_2} \int_{-\infty}^{+\infty} \int_{-\infty}^{+\infty} E_1'(x, y, d, z_1, t)$$
$$\exp\left\{-\frac{jk}{2z_2}\left[(x_2 - x)^2 + (y_2 - y)^2\right]\right\} dxdy \tag{6}$$

in which λ and $k = 2\pi/\lambda$ are the wavelength and the wave number of the probe beam, respectively, z_2 is the distance from the sample to the detection plane, (x, y) and (x_2, y_2) are the coordinates in the sample and detection plane, respectively, and $E'_1(x, y, d, z_1, t)$ is the complex amplitude of the electric field of the probe beam at the exit plane of the TL element, that is,

$$E_1'(x, y, d, z_1, t) = E_1(x, y, z_1) exp[-j\Delta\Phi(x - d, y, t)] \tag{7}$$

$E_1(\cdot)$ and $\Delta\Phi(\cdot)$ are the electric field of the probe beam before the TL element and the phase change induced by the TL element, respectively. For a Gaussian probe beam with TEM00 mode, $E_1(\cdot)$ can be found in Liu et al. (2012).

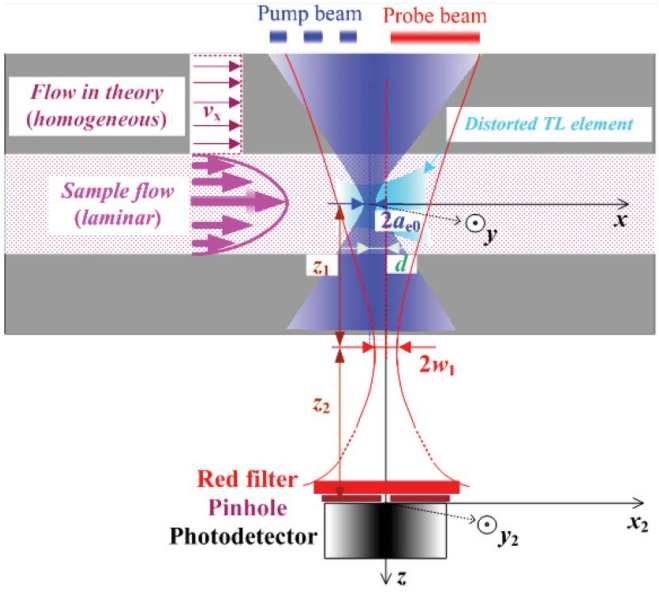

FIG. 3. Schematic diagram of the optical configuration of a TLM system in a microchannel (from Liu et al., 2013). © 2013 Springer. Reproduced by permission of Springer. Permission to reuse must be obtained from the rightsholder.

For the collinear TLS,

$$\Delta\phi(x-d,y,t)=\frac{2\pi}{\lambda}l\frac{dn}{dT}T(x-d,y,t) \quad (8)$$

When using a photodiode placed behind a pinhole to measure the axial intensity of the probe beam, the TL signal S can be defined as

$$S=\frac{S_{ac}}{S_{dc}}=\frac{|E_2(t=n/f+1/(2f))|^2-|E_2(t=n/f)|^2}{|E_2(t=0)|^2} \quad (9)$$

where S_{ac} is the intensity change of the probe beam in a modulation cycle corresponding to the modulation frequency (f), n is an arbitrary cycle in steady state, and S_{dc} is the central intensity of the probe beam before excitation.

In the derivation above, only the impact of the sample flow on the TL signal was considered. When the sample length is much larger than the confocal distance of the pump laser ($z_{ce}=2\pi {a_{e0}}^2/\lambda_e$, with λ_e the wavelength of the pump beam), the influence of the pump beam divergence should be included (Liu and Franko, 2013). When the sample length is comparable to or smaller than the confocal distance of the pump laser, the impacts of the top/bottom layers of the sample cell on the TL signal should be taken into account (Liu et al., 2012). When z_1 is comparable to or even smaller than the thickness of the TL element (usually the case in laser-excited TLM), there exist different z_1s for different thin TL elements (if we treat this "thick" TL element as a combination of many thin TL elements), and a "finite TL element"-based model was used to calculated the TL signal as the sum of TL signals of N thin TL elements (Liu and Franko, 2013). When the pump beam waist is comparable to the size of the sample cell, the impact of sidewall on the TL signal should be considered (Bialkowski and Chartier, 2001; Chartier and Bialkowski, 1997; Liu et al., 2012).

In addition, influences of some other factors should also be considered where necessary, such as absorption saturation (Georges et al., 1996; Harata, 2007; Ramis-Ramos et al., 1994), transient absorption (Harata, 2007; Harata and Yamaguchi, 2000; Harata et al., 2002), absorbance change during chemical reactions (Franko and Tran, 1991a, 1991b; Malacarne et al., 2011; Pedreira et al., 2006), matrix effects (Georges, 2008), and Soret effect (Cabrera et al., 2009).

INSTRUMENT DEVELOPMENT AND APPLICATIONS

Although TLM has exclusive advantages of fast response, micro space compatibility, and high temporal and spatial resolution over TLS system, its sensitivity is still over 10 times lower than that of the TLS due to the much shorter sample length in the microchannel, such as 100 μm in contrast to 1 cm in a TLS system. Therefore, increasing the sensitivity of TLM as well as lowering the instrumental noises is always one of the most important tasks for instrument development. On the other hand, to improve the general disadvantage of TLS systems, namely its specificity, multiple laser lines from UV, to visible to near-infrared (NIR) or even broadband incoherent light sources were used as the excitation source. Furthermore, to meet special detection requirements or applications, some new TLM apparatuses (CD-TLM, PM-TLM, DIC-TLM) were developed as well.

Improvements for Lower Limits of Detection

To obtain the lowest limit of detection (LOD), systematic parameters including the optical configuration, sample solvent, and noises were optimized.

Optical Parameters

One of the optical parameters closely related to the TL signal is the excitation power density, which is determined by the pump beam power and beam radius in the sample. According to the enhancement factor ($\theta=P(-\partial n/\partial T)/(k\lambda)$), one direct way to increase the sensitivity is to enhance the power of the pump beam. However, at high powers, nonlinear absorption (Marcano O. et al., 2011), convective noise (Georges, 1999) (although it is not as pronounced in a microchannel as in an ordinary cell; Proskurnin et al., 2003), optical saturation (Georges et al., 1996; Ramis-Ramos et al., 1994), and multiphoton processes (Bindhu et al., 1999; Taouri et al., 2009), or light-induced damage to the analyte, especially for some biological molecules (Chen et al., 2002; Takeshita et al., 2003), could occur. Alternatively, decreasing the pump beam radius in the sample can also enhance the TL signal as in case of TLM, but the possible nonlinear absorption or light damage to the analyte should be considered as well. Furthermore, selecting a probe beam with shorter wavelength increases the sensitivity. Increasing the probe beam power can enhance the absolute TL signal amplitude and subsequently decrease the LOD when the noise in the TLS system is mainly the shot noise. In addition, increasing the effective sample length is also a way to enhance sensitivity.

At given pump beam parameters (power, beam radius), the second strategy is to optimize the optical configuration of the pump and probe beams, including the arrangement of the pump and probe beams (collinear, quasi-collinear, or crossed-beam), the mode mismatching degree, the probe beam radius at its waist, and the signal generation mechanism (by diffraction or interference).

As the typical optical configuration, collinear TLS has been extensively developed in the past and is the only possible configuration in TLM because of spatial constraints for relatively large optical elements. As shown in Figure 4 (Liu et al., 2013), the excitation beam, which can be derived from a laser or other light sources, and the probe beam are tightly focused onto the sample by an objective lens (OL). For the laser-excitation case, the beam waist radius in the sample is usually

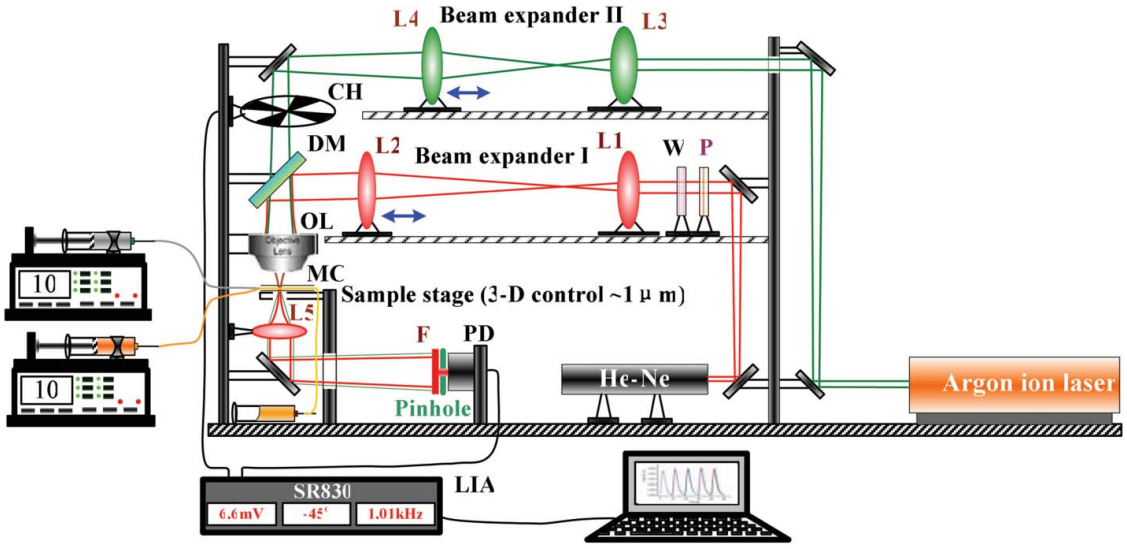

FIG. 4. Schematic diagram of a laser-excited TLM coupled with a microfluidic system. CH: mechanical chopper; DM: dichroic mirror; F: interference filter at 632.8 nm; L1–L5: lenses; MC: microchip; OL: objective lens; P: linear polarizer; PD: photodiode; W: $\lambda/4$ wave plate at 632.8 nm (from Liu et al., 2013). © 2013 Springer. Reproduced by permission of Springer. Permission to reuse must be obtained from the rightsholder.

$\sim$1 μm. Due to the chromatic aberration of the OL or by using a beam expander (beam expander I, Figure 4) before the OL, mode-mismatching between the pump and probe beams is realized for high sensitivity. In the far-field detection scheme, the TL signal is monitored by a photodiode.

In early-stage TLM instruments, it was believed that, as in conventional TLS (Sheldon et al., 1982), the maximum TL signal occurred at $z_1 = \pm\sqrt{3}z_R$ ($z_R = \pi w_1{}^2/\lambda$: Rayleigh range of the probe beam, with w_1 the beam waist radius of the probe beam) and was generated mainly within the confocal distance ($z_{ce} = 2z_{Re}$, with $z_{Re} = \pi a_{e0}{}^2/\lambda_e$) of the pump laser (Kitamori et al., 2004). However, it was later found experimentally that the signal-contributing volume was larger than the confocal distance, such as in Proskurnin et al. (2003), where an effective path length of 13.5 μm at the pump beam waist radius of 0.68 μm was estimated in comparison with the confocal distance of 5.6 μm, while in Li et al. (2007), the entire cell length of 100 μm contributed the TL signal in comparison with the confocal distance of 9.3 μm at the pump beam waist radius of 1.2 μm. For the optimum distance of z_1, although a reasonable conclusion that the optimum optical scheme occurred when the probe beam diameter fitted the diameter of the thermal lens was obtained, the value of the mode-mismatching degree m ($= (w_s/a_{e0})^2$, with $w_s = w_1[1 + (z_1/z_R)^2)]^{1/2}$ being the probe beam radius in the sample plane) of 3 and the resulting z_1 of $0.6z_R$ were underestimated due to the use of an approximate temperature model (Smirnova et al., 2008). In Li et al. (2007), the optimum z_1 was obtained at $5z_R$. To unify the above discrepant conclusions, a more general and accurate theoretical model was built on the basis of the Fresnel diffraction theory (Liu et al., 2012), where the influences of the pump beam divergence, sample flow, top/bottom layers, and sidewall of the sample cell on the TL signal were taken into consideration. For a TL element with thickness comparable to or larger than z_1, a refined TLS model was developed (Liu and Franko, 2013). In comparison with the model in Liu et al. (2012), where the thickness of the TL element is treated as infinitesimal, this model approximates the TL signal as the sum of TL signals of N thin TL elements, which is expressed as

$$S_{tl} = \sum_{i=1}^{N} \frac{\left|E_2(r_2, z_1(i) + z_2, t = n/f + 1/(2f))\right|^2 - \left|E_2(r_2, z_1(i) + z_2, t = n/f)\right|^2}{\left|E_2(r_2, z_1(i) + z_2, t = 0)\right|^2} \quad (10)$$

For the ith thin TL element, $z_1(i) = -z_0 + z_i$, is the distance from the probe beam waist to the center of the ith thin TL element. In $z_1(i)$, z_0 is the position of the probe beam waist relative to the first thin TL element and is negative when the probe beam waist is located to the left of the first thin TL element, as presented in Figure 5, and $z_i = (2i\text{-}1)l/(2N)$. Both theoretical simulations and experimental results showed that for a 100 μm deep microchannel ($H_c = 100$ μm) at $f = 1$ kHz, the optimum z_1 was obtained at around 105 μm for $a_{e0} = 2$ μm and at 75 μm for $a_{e0} = 0.7$ μm, and the corresponding mode-mismatching degrees were 100 and 400, respectively, and the effective light path length (L_{eff}) was $6z_{ce}$ ($L_{eff} = 293$ μm at $a_{e0} = 2$ μm and 35.9 μm at $= 0.7$ μm, $\lambda_e = 514.5$ nm) (Liu and Franko, 2013). When $H_c < L_{eff}$, $l = H_c$, otherwise $l = L_{eff}$. We need to note that the above values of z_1 and l were

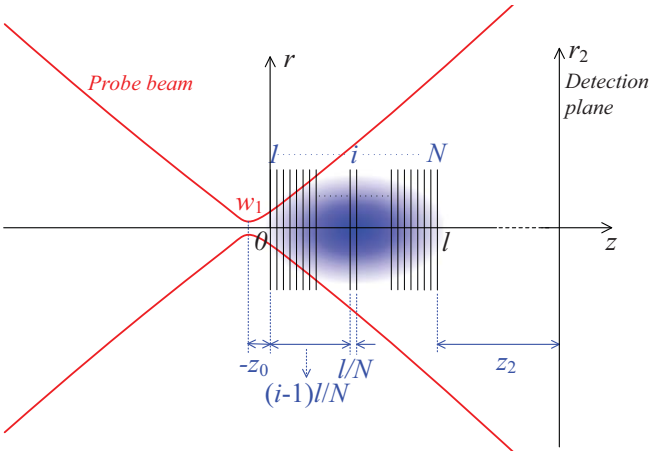

FIG. 5. Schematic diagram of the optical configuration of a typical laser-excited TLM, where a probe beam is diffracted by a finite TL element (represented by a series of N thin TL elements) (from Liu and Franko, 2013). © 2013 Springer. Reproduced by permission of Springer. Permission to reuse must be obtained from the rightsholder.

obtained at given pump beam waist radius a_{e0} of 2 or 0.7 μm, modulation frequency of 1 kHz, and sample length of 100 μm. If the pump beam waist radius is smaller and/or the modulation frequency is higher and/or the sample length is shorter, the optimum z_1 and effective sample length will be smaller. For a given microchannel depth, a conclusion, which can be generalized to any TLS setup, is that the maximum TL signal appears at an optimum beam size where the confocal distance of the pump beam is approximately half of the microchannel depth or sample thickness, namely:

$$a_{e0} = \sqrt{\frac{\lambda_e H_c}{4\pi}} \tag{11}$$

After optimization of the beam parameters for laser-excited TLM the achieved LOD of 8.6×10^{-9} M for ferroin in a 100 μm microchannel at an excitation power of 4 mW is 2.3 times lower than that reported by Proskurnin et al. (2003), where a LOD of 2×10^{-8} M was reached by using a 10 times higher excitation power. The improvement in LOD can be attributed partly to the optimization of the optical configuration, and partly to the possible difference in the performance of the components (such as stability of lasers, detector noise) used in the two TLM systems.

For flowing samples, the collinear TLM discussed above can be used without any change if the flow velocity is low (such as less than 1 cm/min), otherwise one of the beams (usually the pump beam for convenience) should be displaced a certain distance, as in TLS systems (discussed above), to compensate for the change of the temperature distribution. For low flow velocities, Li et al. (2007) developed a collinear-beam TLM detector and introduced it into a high-performance liquid chromatography (HPLC) system (mobile phase: 80% methanol and 20% deionized water) to analyze a mixture of five anthraquinone dyes and got LODs of 0.5–1.2 μg/L with a path length of 200 μm at a pump power 28 mW. For the case of higher flow velocities, the initial collinear arrangement of the pump and probe beams has been to some extent misaligned on purpose by displacing one of the beams to compensate for the change of the temperature distribution, and we can call this configuration quasi-collinear TLM. Through displacing the beams to an optimum distance (d_{opt}), which, for example, is theoretically calculated to be $0.6a_{e0}$ at $v_x = 5$ cm/s and $f =$ 1 kHz, the TL signal achieved maximum for every selected flow velocity from 1 to 10 cm/s, and a better response linearity of TLM was shown over three orders of magnitude of sample concentration (Liu et al., 2013). To what extent the sample flow influences the TL signal depends on how the heat is moved away in a modulation cycle and how the temperature distribution deteriorates, which is determined by the flow velocity, the modulation frequency, and the pump beam radius. For the excitation by a point-like pump beam (such as the diffraction-limited pump beam under a high-numerical-aperture OL) (Liu et al., 2012), the TL signal is slightly changed by the sample flow when the translational distance L_f of the fluid in an excitation or cooling duration ($L_f = v_x/(2f)$) is smaller than the thermal diffusion length ($D_{th} = [D/(\pi f)]^{1/2}$) and will decrease when L_f is larger than D_{th}. The higher the flow velocity, the bigger the signal decrease will be. When the pump beam waist radius is larger than D_{th} and/or when the modulation frequency is low, sample flow below certain limit (such as $L_f < a_{e0}$) will increase the TL signal to a certain extent because of the heat aggregation resulting from a coupled effect of laser-induced heating, thermal diffusion, and flow-induced heat translation at a certain area within the detection volume of the probe beam (Liu and Franko, 2014a; Liu et al., 2012; Smirnova et al., 2008).

Besides the influence of the sample flow, photostability of the sample also impacts the TL signal (Liu and Franko, 2014a, 2014b; Mawatari et al., 2008; Ragozina et al., 2002). Some works have shown that for photolabile samples, the TL signal will first increase with flow velocity and then decrease with further increase of the flow velocity. The maximum signal occurred at a certain flow velocity where a compromise is made between the less photodegradation-resultant signal improvement and the flow-induced signal decrease. As shown in Liu and Franko (2014b), this flow rate occurred at about 10 μL/min (corresponding to 2 cm/s in a 200 μm wide $\times$ 50 μm deep microchannel) for Cr-DPC complexes (obtained after reaction of hexavalent chromium (Cr) with diphenylcarbazide (DPC)) at an excitation power of 60 mW and pump beam waist radius of 2 μm. The critical number of photons absorbed by a single Cr-DPC complex, above which the molecule will be photodegraded, was calculated to be about 4000. Further increasing the carrier flow rate up to 20 μL/min

allowed recording analytical signals for 12 sample injections in one minute although the TL signal decreased a little bit by the liquid flow. This provides a solid basis for further realization of high-sample-throughput analysis.

To realize precise positioning of the light beams with respect to the microchannel, a portable TLM with a focusing system was developed (Mawatari et al., 2005). The astigmatism of the reflected excitation beam from the microchip was used for depth direction focusing, and the scattering effect of the transmitted probe beam by a microchannel edge was used for width direction focusing. The focusing system was evaluated with a 250 μm wide $\times$ 50 μm deep microchannel. Focusing resolutions for depth and width directions were 1 and 10 μm, respectively. The same authors then developed a reflective portable TLM (Mawatari and Shimoide, 2006). An aluminum mirror was deposited on the main plate of the microchip to reflect the probe beam back to a detection unit. One possible problem in this instrument is the background signal due to light absorption of the aluminum mirror, which was reduced 60 times by spacing the microchannel and the mirror by 600 μm. A quadrant photodiode was used to regulate the tilt angle of the microchip within $\pm$ 0.05°. The LOD was 60 nM for xylene cyanol solution, corresponding to an absorbance of 9.4×10^{-6} AU about 40 times lower than with a spectrophotometer.

In addition, to meet special detection requirements or applications, some new TLM apparatuses were developed by changing the excitation mode or by miniaturization, which leads to final commercialization.

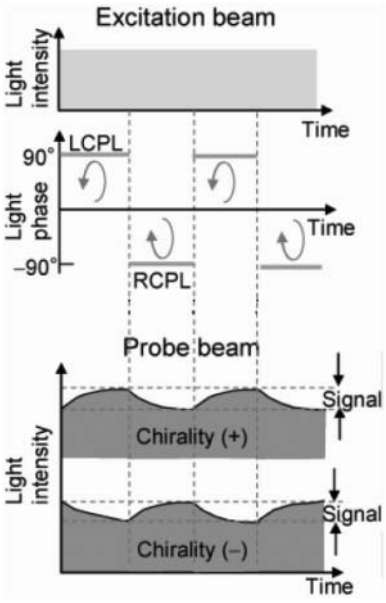

FIG. 6. The principle of a CD-TLM (from Yamauchi et al., 2006a). © 2006 American Chemical Society. Reproduced by permission of the American Chemical Society. Permission to reuse must be obtained from the rightsholder.

To measure chiral samples, a circular dichroism TLM (CD-TLM) was proposed (Yamauchi et al., 2006a), in which by analogy to previous work on CD-TLS (Xu and Tran, 1990a, 1990b), the differential light absorption between left-circularly polarized light (LCPL) and right-circularly polarized light (RCPL), as shown in Figure 6, was detected as TL signal intensity and phase. The LOD for enantiopure $[(\text{-})\text{Co-(en)}_3]^{3+}\text{I}_3^-$ was 6.3×10^{-5} M (1.9×10^{-7} AU), which was more than 250 times lower than that in a CD spectrophotometer. Then, CD-TLM was extended to the UV region to measure aqueous solutions of optically active camphorsulfonic acids (CSA) (Mawatari et al., 2008). Since the sample could be photochemically decomposed by UV pulsed laser irradiation, a flow velocity of 10 mm/s was selected for higher sensitivity. The LODs of 8.7×10^{-4} M ($\Delta A = 5.2 \times 10^{-6}$ AU) for (+)-CSA and 8.4×10^{-4} M ($\Delta A = 5.0 \times 10^{-6}$ AU) for (−)-CSA were obtained.

Conventional laboratory-built TLM entails use of large-scale lasers and many optical components, so it is still a large-scale detection system, which lacks portability and requires specialized operators. Yamauchi and coworkers (Tokeshi et al., 2005; Yamauchi et al., 2006b) developed a miniaturized TLM system for microchip chemistry. The system is composed of laser diode modules, fiber-based optics combined with an objective Selfoc microlens (a gradient index lens, characteristics of which can be controlled arbitrarily by changing ion species, spatial distribution of implanted ions, and lens height), as shown in Figure 7, and miniaturized detection units for TL signals. In a microchip with channel depth of 200 μm, the detection limits were 5.6 μg/L for Ni(II) phthalocyanine tetrasulfonic acid at $P = 3.4$ mW and 2.4 μg/L for cy5 (a fluorescent dye from the cyanine dye family) at $P = 0.6$ mW. Recently, Mawatari et al. (2011b) constructed a TLM similar to that of Yamauchi et al. (2006b), but they used a focusing

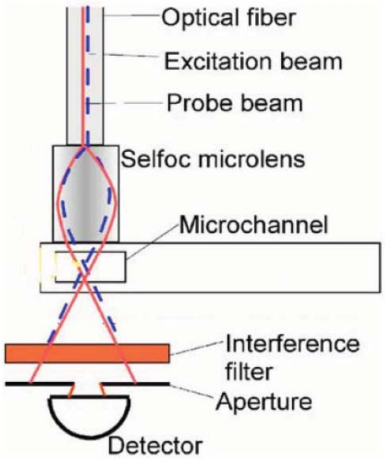

FIG. 7. Miniaturized thermal lens system with Selfoc microlens as the focusing lens (from Yamauchi et al., 2006b). © 2006 Elsevier. Reproduced by permission of Elsevier. Permission to reuse must be obtained from the rightsholder.

lens (composed of a combination of three microlenses) as an alternative to the Selfoc microlens, and employed a custom-made lock-in amplifier to further minimize the device. The LOD was 10 nM for nickel(II) phthalocyaninetetrasulfonic acid tetrasodium salt solutions (corresponding to an absorbance of 9×10^{-6} AU). Though these systems are very small, the detection limits cannot reach as low as in a conventional TLM since optimization to the optical configuration, such as the mode-mismatching degree, was limited by the chromatic aberration of the focusing lens, the transmitted power was attenuated by the fiber, and also the wavelength tunability of these instruments is quite limited due to the use of fibers to transmit both the pump and probe beams and the use of the chromatic aberration of the focusing lens to realize a mode mismatching.

A commercial desktop-size TLM (DT-TLM), the ITLM-10 (Institute of Microchemical Technology Co., Ltd.; http://www.i-mt.co.jp/), as a compromise in detection limit, wavelength tunability, and compactness between conventional and fiber-based TLMs, has recently been developed by introducing compact diode lasers and miniaturized opto-mechanical components. As an improvement to ITLM-10, Smirnova et al. (2012) proposed a near-field DT-TLM. Strictly speaking, the use of "near field" is inaccurate in this case. In optics, the detection point is in the "near field" when the Fresnel number ($F_n = a^2/(\lambda z)$, with a the radius of the diffractive element and z the distance from the element to the detection point) is above 1 or in the "far field" when $F_n < 1$ (Voelkel and Weible, 2008). All the present TLMs employ a far-field detection scheme since the Fresnel number of the TLM system is much smaller than 1. For example, $F_n = 0.002$ for a 632.8 nm probe beam diffracted by a 10 μm-size TL element at a detection distance of 2 cm. Compared with the ITLM-10, the following changes were made in the new DT-TLM: (1) instead of a large-scale beam expander, a compact expander consisting of two microlenses was mounted on the excitation laser head; (2) a focus control was applied to the probe beam (a focusable laser diode on which a long-focal-length plastic lens was mounted), which made it suitable for long-distance and alignment applications; (3) a larger chopper blade was used, which reduced frequency fluctuations from about 10% to 1%; (4) the condenser lens in ITLM-10 was removed and the photodiode was moved to a much closer detection site (3–4 cm from the sample). The improved DT-TLM showed better response linearity and a lower LOD of 3.5×10^{-7} AU for a 50 μm deep microchannel at $P = 50$ mW, representing a 20-fold improvement over ITLM-10.

Though different types of collinear TLM systems have been developed for detection in micro space as stated above, another two types of TLS setups, namely differential TLS and phase-conjugate TLS (Erskine and Bobbitt, 1989; Franko and Bicanic, 1998; Plumb and Harris, 1992; Proskurnin and Volkov, 2008), have still not been applied for detection in micro space. Developing differential or phase-conjugate TLM in the future could expand the application of TLS in micro space for detection of analytes in high background absorption solvents or of optically inhomogeneous samples. Besides detecting analyte, TLM can also be used for determining the reaction parameters, such as stability constants, kinetic constants, and acid dissociation constants, as with conventional TLS (Proskurnin et al., 2005b).

The above-discussed collinear TLS is usually applied to sample cells or microchips with flat sample cell walls, which almost don't change the beam profile of the probe beam and subsequently facilitate the alignment/optimization of the optical configuration behind the OL. When the sample cell has a round wall, such as in capillaries used in capillary electrophoresis (CE), the alignment and optimization will become difficult if the pump and probe beams propagate through the same OL since the round wall changes the fringe pattern of the probe beam and an iterative procedure is required for the optimization of the TL signal (Chanlon and Georges, 2002). Furthermore, the sensitivity and reproducibility will be reduced by the complicated refraction, reflection, and scattering of the two laser beams on the capillary surface.

To solve this problem, one way is to introduce the compounds separated by CE into an extended microchannel that has flat surfaces (Otsuka, 2007; Uchiyama et al., 2003, 2005) so that the collinear TLS can be used as usual. This method necessitates fabricating an interface on a chip to connect the capillary and the microchannel, which complicates the detection system and could introduce a dead volume posing potential adverse impacts (such as broadening of the CE peaks, cross contamination between samples) on the measurement.

Another way is to use crossed-beam TLS, which is applicable to small-volume detection. The optical configuration of the crossed-beam TLS in a capillary is schematically depicted by Figure 2(a). The sensitivity of this method is expected to be independent of the path length and inversely proportional to the excitation beam spot size. For short pulsed laser excitation (such as ~ns pulse duration), offsetting the pump and probe beams is not necessary, and the peak signal is almost independent of the flow rate since the signal rise is determined by the acoustic transit time, which can be 1,000 times shorter than the thermal time constant. In a capillary with an internal diameter of 75 μm, a LOD of 5×10^{-7} AU was obtained for cobalt nitrate in ethanol under excitation of a Nd-YAG laser operating at 532 nm with pulse energy of 200 μJ (Chanlon and Georges, 2002). For continuous laser-excited TLS, Proskurnin et al. (2005a) optimized a near-field crossed-beam TL system for CE. Under the optimized instrumental parameters ($a_{e0} = 3.88$ μm, $w_1 = 18.5$ μm, $m = 93$, $f = 70$ Hz), the LODs for 2-, 3-, and 4-nitrophenol were $\sim 10^{-6}$–10^{-7} M under excitation of a multimode He-Cd laser working at 325 nm and 50 mW. Dependence of the TL signal on the flow velocity was found to be similar to the case of collinear TLS, namely, the TL signal first increases with flow velocity to a maximum value at about 12 cm/min and then decreases with further increase of

flow velocity. The same authors then investigated the influence of organo-aqueous separation buffers on the TLS measurement in CE separations (Bendrysheva et al., 2006). Taking into account both the signal enhancement due to an improvement in the thermo-optical properties of the separation buffer (70% v/v acetonitrile) and the increase in baseline noise, LODs for 2-, 3-, and 4-nitrophenols were obtained as 1×10^{-6}, 1×10^{-6}, and 3×10^{-7} M, respectively, which were decreased by a factor of six compared to TL detection in aqueous separation buffers. A near-field TL system at 257 nm was used for detection of nitroaromatic compounds in contaminated water after separation by micellar electrokinetic chromatography (MEKC; Ragozina et al., 2002). The LODs for the compounds were $\sim$0.1 mg/L, which showed 30-fold improvement over conventional UV-photometric detection. By using optical fibers to transmit the pump and probe beams, a more compact TL detector for CE was constructed to detect amino acids with LODs of $\sim 10^{-7}$ M (Seidel and Faubel, 1998).

To detect analytes with an absorption band outside the emission line of the pump laser, an indirect TL system with a 325.0 nm He-Cd excitation laser was used in combination with CE for detection of organic anions (Nedosekin et al., 2007). Optimization was made for the selection of background electrolyte (probe ion), probe ion concentration, and modulation frequency. With 50 μM of Mordant Yellow 7 (an azo dye) as probe ion, LODs for 1-heptane-, 1-pentane-, 1-butane-, 1-propane-sulfonic acids, and acetic acid at a level of 0.5–1.1 $\times 10^{-6}$ M were achieved.

The above discussed TLM systems employed the typical TL signal generation mechanism, namely, a probe beam is diffracted by a modulated or pulsed pump beam-induced TL element and its axial intensity change is recorded by a photodetector. These instruments are further referred to as conventional TLMs. Conventional TLMs have offered the possibility of determining a concentration corresponding to 0.4 molecules in a detection volume of 7 fL (Tokeshi et al., 2001b) and counting individual metallic nanoparticles (Mawatari et al., 1998). However, counting individual nonfluorescent molecules is still a difficulty for conventional TLM due to its relatively high LOD induced by the low frequency fluctuation (around 1 kHz) of the probe beam intensity. This probe beam background fluctuation affects the LOD to a greater extent than the background signals originating from the solvent, fluorescence, or other sources. To alleviate the background fluctuation, a differential interference contrast (DIC) TLM was developed (Shimizu et al., 2009). In DIC-TLM, as shown in Figure 8, the probe beam is separated by a DIC prism into two beams with perpendicular polarization, whereas the excitation beam is not separated and it overlaps with one of the two probe beams. Phase contrast appears between the two probe beams due to the difference in refractive index. By optimizing the shear value of the DIC prism to about 5 μm, the probe beam collinear with the pump beam experiences TL-induced phase change, while the other probe beam barely experience this kind of phase change. Then, the probe beams are combined again by another DIC prism, which results in a new polarization component. After removing the initial polarization component using a polarization filter, background-free photodetection is achieved by detecting only this new component with an avalanche photodiode. The background was reduced to 1/100 by differential interference, and the signal-to-background ratio (S/B) was improved by one order of magnitude. This DIC-TLM instrument can perform measurements in concentration determination mode and/or in particle/molecule counting mode. Counting of individual gold nanoparticles (5 nm) was demonstrated by this system. Later, the same authors applied this instrument for determination of the concentration of nonfluorescent species in an extended nanochannel where a LOD of 2.4 μM of Sunset Yellow dye, corresponding to 390 molecules in the detection volume of 0.25 fL, was achieved in a 21 μm wide $\times$ 500 nm deep nanochannel (Shimizu et al., 2010), and in extended nanochromatography

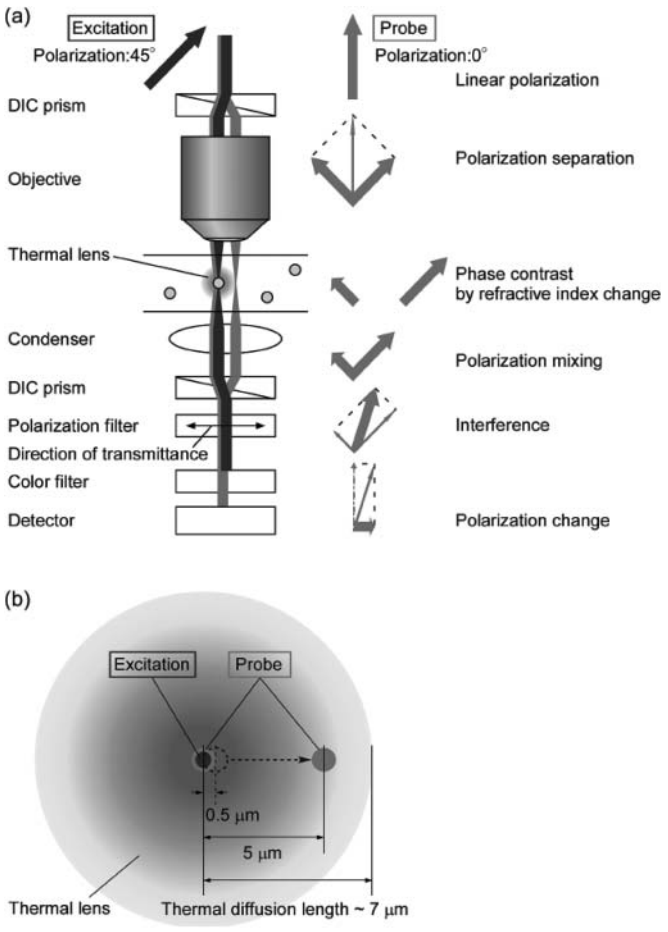

FIG. 8. (a) Principle of DIC-TLM; (b) configuration of beam spots and thermal lens in the focal plane (from Shimizu et al., 2009). © 2009 American Chemical Society. Reproduced by permission of the American Chemical Society. Permission to reuse must be obtained from the rightsholder.

where the LOD was ~10 μM, corresponding to ~1000 molecules in the detection volume of 0.25 fL (Shimizu et al., 2011).

Though much lower probe beam background noise was observed, there is still no report of counting individual nonfluorescent molecules. This is most probably because the presented DIC-TLM didn't achieve a LOD low enough to enable it to detect a molecule with an absorption cross section of $\sim 10^{-16}$ cm^2 two orders of magnitude lower than that ($\sim 10^{-14}$ cm^2) of the gold nanoparticles. When performing experiments with the DIC-TLM, we still need to note the following aspects: (1) The methodological sensitivity is low, especially for analytes with low absorption cross sections and corresponding molar extinction coefficients, and the response linearity is not good (around one order of magnitude). An avalanche photodiode, which is used to amplify the incident photon-generated photocurrent, is not just more expensive than conventional photodetectors, but more importantly it introduces additional noises and the output linearity is also limited due to the avalanche process (this further limits the response linearity). (2) In contrast to conventional TLM, which is only slightly influenced by light scattering background, the DIC-TLM instrument is sensitive to any phase-changing factors. Besides the analyte-induced TL, other factors such as some alien particles and nonuniformity of solutions and/or surroundings with different thermophysical properties (Shimizu et al., 2010) would introduce error to the detection or decrease detection sensitivity. (3) With more optical components (polarizers, prisms, wave plates) and more complicated optical configuration than conventional TLM, the alignment is very complex and would be different for solutions with different thermophysical properties since the required optimum shear value of the prism is different.

Selection of Solvent

As defined by the enhancement factor, TL signal is proportional to the ratio $(dn/dT)/k$. Therefore, choosing an appropriate solvent with larger dn/dT and smaller k will increase the sensitivity of TL measurements. Organic solvents have much higher dn/dT and lower k than water. Addition of water-mixable solvents such as acetonitrile to the eluent and postcolumn reagent (30% and 60% v/v, respectively) enabled simultaneous determination of Cr(VI) at 0.1 μg/L and of Cr(III) at 10 μg/L levels by ion chromatography (IC) with TLS detector (Šikovec et al., 2001). The addition of acetonitrile provided 5.4 times higher enhancement factor than an aqueous eluent. In CE, LODs for 2-, 3-, and 4-nitrophenols in 70% v/v acetonitrile separation buffers were decreased by a factor of six compared to aqueous separation buffers (Bendrysheva et al., 2006). The thermal conductivities of organo-aqueous mixtures k_m were calculated by the Filippov equation:

$$k_m = x_a k_a + x_o k_o - 0.72|k_o - k_a| x_a x_o \qquad (12)$$

where x_a and x_o are the mass fractions of water and organic solvent, respectively. The $(dn/dT)_m$ values were calculated as a linear combination of the molar fractions:

$$(dn/dT)_m = v_a (dn/dT)_a + v_o (dn/dT)_o \qquad (13)$$

where v_a and v_o are the molar fractions of water and organic solvent, respectively.

The type and quantity of organic solvents added into separation buffers or mobile phase in separation techniques (HPLC, IC, CE) or carrier liquids and reagents in microfluidic chips should be selected by considering not just a high enhancement factor, but more importantly the impact of the solvent on the analyte, separation efficiency, and baseline noise (Bendrysheva et al., 2006; Nedosekin et al., 2007). It was found that the reproducibility of measurement by a TLS system in organic solvents was a few times worse than in water (Proskurnin et al., 2004). Many bioanalytical assays cannot be performed in organic solvents due to denaturation of biomolecules (Franko, 2009).

Room-temperature ionic liquids (RTILs) also provide a better medium for TLS measurements than water. RTILs can offer over 20 times higher sensitivity than water, and the enhancement could even be adjusted by changing the cation and/or the anion in the ILs (Tran et al., 2005). RTILs could therefore be used in various analytical systems combined with TLS detection to replace either water or volatile organic solvents. However, ILs at concentrations of just 1% in aqueous solution were shown to cause inhibition of acetylcholinesterase (AChE) and therefore cannot be used for sensitivity enhancement when AChE or similar enzymes are used (Boškin, 2008). It has, however, been shown for chloroperoxidase that its activity is preserved in some ILs, even at 30% addition of ionic liquid (Boškin et al., 2009).

For a given TLS system, the real analytical efficiency is primarily determined by reaction conditions. Proskurnin et al. (2011) pointed out that as green analytical solvents, aqueous solutions modified with surfactants (such as water-soluble polymers) provide more efficient optimization of reaction conditions than organo-aqueous solutions. They are commercially available and inexpensive and can be used as both single-phase and extraction two-phase systems. High photothermal sensitivity in these solutions positions them as an alternative to organic solvents for increasing TLS sensitivity in aqueous media (Tran and Van Fleet, 1988).

Apart from the above methods, other possible ways for sensitivity enhancement have also been developed, such as using on-line sample preconcentration (Kitagawa et al., 2006; Otsuka, 2007), reversed micelles (Tran, 1988), crown ethers (Tran and Zhang, 1990), unique properties of water (Franko and Tran, 1989), sample matrix absorption of the probe laser beam (Grishko et al., 2002), and even the latest reported, laser-induced precipitation (Nedosekin et al., 2009).

Noises

In TLS systems, there are mainly two kinds of noise sources.

One is light irradiation-induced detector noises or inherent electronic noises of the detector and cables such as thermal noise, shot noise, and flicker (1/*f*) noise, in which 1/*f* noise can be reduced by performing TLS measurement at high modulation frequency. Flicker noise is directly proportional to the light intensity, while shot noise increases with the square root of light intensity.

The other is noise caused by the fluctuation of the probe beam intensity in the detection plane. On one hand, this may be induced by the pump and probe lasers, such as fluctuation of the pump laser power, which can be reduced by real-time recording of the power change and accounting for it in the TL signal; mode instability (especially for pulsed laser) and pointing noise of the pump laser; and the power fluctuation and beam pointing instability of the probe laser. The impact from beam pointing instability of the probe laser can be lessened by employing a larger pinhole, and that from power fluctuation of the probe laser can be corrected by employing differential detection (Kachanov, 2008). On the other hand, the noise can be caused by the convection or flow of the sample and/or indirectly by the background absorption of the solution. Therefore, in flowing mode, a stable pump should be used to assure a constant flow. For solvents or samples with high background absorption, the absolute noise increases proportionally. Therefore, selection of appropriate blank or carrier solution, and/or derivatization reagent if derivatization is necessary, is of particular importance to assure low noises. As demonstrated for the determination of Fe(III) and Fe(II) ions by IC-TLS (Divjak et al., 1998), colorless reagents, for example, 1,10-phenanthroline, were advantageous and provided two and four times lower LODs than reagents with relatively high background absorbance. In addition, contamination of the microchannel will increase the background signal as well. With increased surface-to-volume ratio in microfluidic devices, contamination of the channel wall by heated or even burnt substances could happen, especially when the excitation power density is high. This could be alleviated by increasing the flow rate and/or using an excitation beam with lower power or power density around the channel wall.

For a TLM system equipped with good-quality lasers (with power instability less than 1%), we investigated the noise and signal-to-noise ratio (*S*/*N*) of the system for detecting 10 μM ferroin aqueous solution at different modulation frequencies and sample states, as shown in Figure 9. In a static sample cell, we found that the change of the noise with different pinhole aperture-to-beam size ratios ($d_{ph}/(2w_2)$) agreed with the predictions of Erskine and Bobbitt (1988). At modulation frequencies over 1 kHz (Figure 9(a)), the noise originated mainly from the shot noise of the probe beam, while at low frequencies, such as 5 Hz (Figure 9(b)), the TLM system is limited by

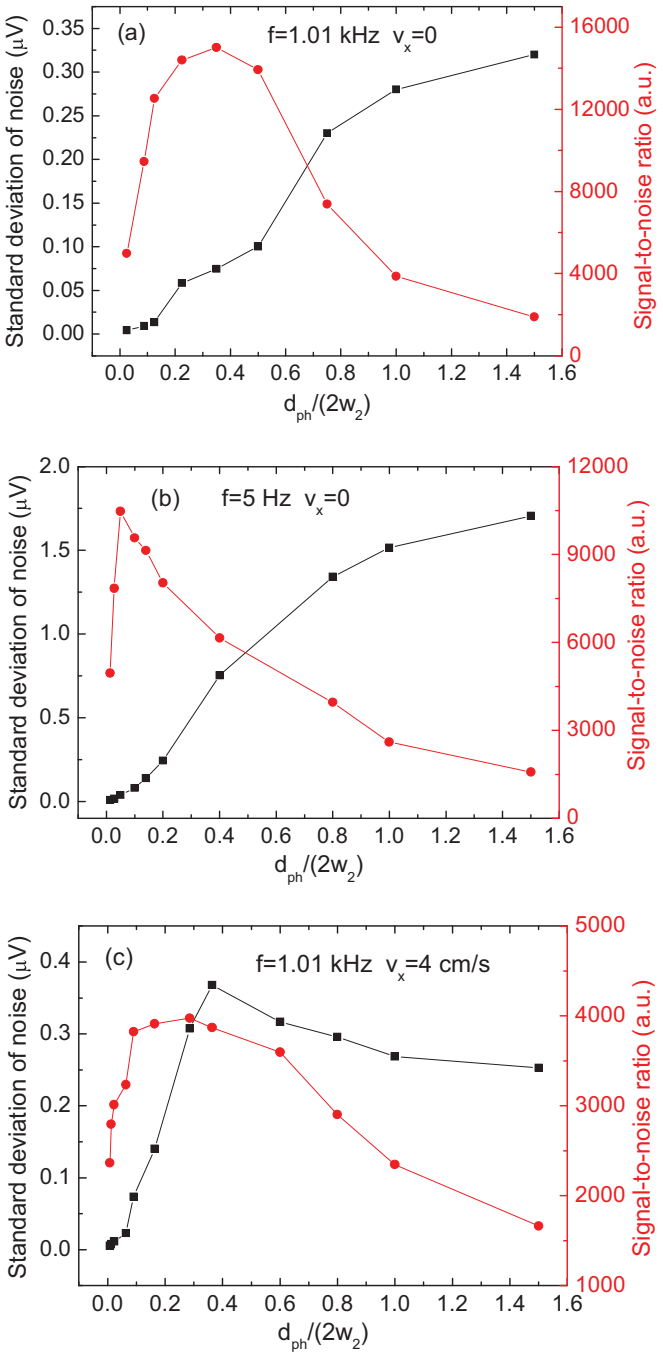

FIG. 9. Probe beam noise level and signal-to-noise ratio as a function of $d_{ph}/(2w_2)$ for the TL system working at (a) f = 1.01 kHz and $v_x = 0$, (b) $f = 5$ Hz and $v_x = 0$, and (c) f = 1.01 kHz and $v_x = 4$ cm/s. The pump beam waist radius is 2 μm and the excitation power is 60 mW.

the flicker noise of the probe beam. The optimum $d_{ph}/(2w_2)$ was found to be about 0.4 at high frequencies (e.g., 1 kHz) and about 0.05 at low frequencies (e.g., 5 Hz). In microfluidic chips, fluctuation of the liquid flow could disturb the

propagation of the probe beam through the microchannel and consequently introduce additional noise. The flow-induced noise behaves like the noise caused by the beam-pointing instability of the light source (Liu et al., 2013). We demonstrated that for water as the fluid, when the flow velocity was less than 1 cm/s, there was little flow-induced noise, and when the flow velocity was high (such as above 2 cm/s), the TLM setup was limited by the flow-induced noise. The value of $d_{ph}/(2w_2)$ could be selected between 0.1 and 0.4 for high signal-to-noise ratio (Figure 9(c)). We also found that the solvent with smaller density and/or viscosity would produce lower flow-induced noise. For example, the noises (N) induced by several commonly used solvents are in the order of N(acetone or acetonitrile) $<$ N(methanol) $<$ N(ethanol) $<$ N(trichloromethane). Further and more detailed investigation of the flow-induced noise by different solvents or mixtures at different modulation frequencies is in progress.

Improvements of Specificity

In TLS instruments, one of the most important parts is the excitation light source. A variety of lasers, ranging from CW gas lasers (e.g., He-Ne (540 nm, 632.8 nm, 1.15 or 3.39 μm), CO (1626–1910 cm^{-1}), CO_2 (880–1090 cm^{-1}), He-Cd (325 nm, 441.6 nm), Ar+ (351.1–1092.3 nm), and Kr+ (406.7–676.4 nm)), dye (320–1200 nm), and semiconductor lasers (380–1650 nm), to Nd:YAG lasers (1064 nm, and higher harmonics 532, 355, and 266 nm), excimer lasers (KrF 248 nm; Qi et al., 1999), and spectrally tunable Ti-sapphire (865 to 1050 nm; Tran and Grishko, 1994) and F-center lasers (2.5 to 3.5 μm; Tran et al., 1994), as well as Er-doped fiber amplifiers (1500 to 1570 nm; Baptista and Tran, 1997), were used for excitation in TLS.

In the visible region, Tran and Simianu (1992) exploited six wavelengths (457.9, 476.5, 488, 496.5, 501.7, and 514.5 nm) emitted by an argon ion laser to periodically excite the sample during a time period of 1.5 seconds. The LOD of such a TLS system is comparable to that of other dual-beam TLS instruments, and it can be used to analyze samples with up to six different components. For determination of various inorganic species (heavy metals, inorganic anions) in the visible region, coloring reagents and ligands such as 1,10-phenanthroline (Divjak et al., 1998), pyridine-2,6-dicarboxylic acid (Šikovec et al., 1995, 2001), 1,5-diphenylcarbazide (Madžgalj et al., 2008; Šikovec et al., 1995, 2001), and 4-(2-pyridylazo) resorcinol (Šikovec et al., 1996) were used for derivatization. However, derivatization is sometimes difficult to perform, especially for small molecules. It might also introduce unexpected interference to the analysis or cause changes of the analyte, so lasers in other wavelength regions were also employed.

In the UV region, a frequency-doubled Ar+ laser was used for detection of nitroaromatic compounds in contaminated water by a crossed-beam TL system at 257 nm after separation by micellar electrokinetic chromatography (Ragozina et al., 2002), and for detection of neonicotinoids by a TLS system at 244 nm after separation by LC (Guzsvány et al., 2007); the third harmonics (261 nm) of a mode-locked Ti: sapphire laser has been used in a TLM for imaging yeast fungus cells (Harata et al., 2007), and the fourth harmonics (214 nm) was employed in a crossed-beam TL system coupled with micro-HPLC for direct detection of non-labeled amino acids (Katae et al., 2010). Hiki et al. (2006) developed a UV-TLM using a high-repetition-frequency (80 kHz) 266 nm UV pulsed laser for detection of nonfluorescent molecules on a microchip. Combined with LC, the UV-TLM enabled separation and detection of fluorene and pyrene with 150 times higher sensitivity than a spectrophotometric method. In the near- and middle-infrared (IR) region, an erbium-doped fiber amplifier (EDFA) combined with an acousto-optic tunable filter (AOTF), tunable from 1500 to 1570 nm, was used in a TLS system for determination of nucleotides (Baptista and Tran, 1997) and a NIR diode laser was used in a TLS system for determination of phosphorus in aqueous phase based on a heteropoly blue method (Nakanishi et al., 1985). In addition, IR radiation between 4000 and 400 cm^{-1} has been utilized in organic structure determination. With the 934.9 cm^{-1} emission line of a CW CO_2 laser, free fatty acids (FFAs) were determined by a TLS system at concentration levels below 1% (Bicanic et al., 1996). At 1734 cm^{-1} of a CO laser (Bicanic et al., 2006), a method combining a TLS system and HPLC discriminated fatty acids from higher concentrations of co-eluting noncarboxylic compounds such as longer chain alcohols (octanol, decanol), which show weak absorbance at the excitation wavelength.

Though offering high sensitivity and low limits of detection, laser-excited TLS is still not used for routine chemical analysis due to its low specificity caused by the limited emission lines of lasers available for excitation. It is, therefore, of particular importance that this restriction be ameliorated. In contrast to lasers, incoherent light sources (ILSs) with top-hat beam intensity profile (Li et al., 2005) have become interesting recently as another kind of light source since they usually have a broad wavelength tuning range. ILSs include electric discharge lamps (halogen-tungsten, xenon, and deuterium arc lamps), light-emitting diodes (LED), among others. Due to the incoherence and low power at a single wavelength, only a few works employed this kind of light source in TLS. Bialkowski and Chartier (Chartier and Bialkowski, 1997) introduced a xenon lamp into a conventional 1 cm sample cell-based TLS and achieved a detection limit of $\sim 10^{-5}$ AU for pseudo-isocyanine dye in ethanol at irradiance of 7.5×10^3 W/m^2. They also introduced photothermal spectrometry in small channels, where the TL element in a liquid is formed by thermal diffusion from the irradiated sample volume through the sample cell walls (Bialkowski and Chartier, 2001). The apparatus has been found to work with cells designed to contain sample volumes from 6 μL down to 24 nL. Marcano O. et al. (2006)

described a white light TL setup for measuring the absorption spectra of dye solutions. This setup used a xenon lamp as the excitation source with a spectral resolution of 10 nm from 400 to 700 nm. A comparison of the TL and absorption spectra of a fluorescent dye (Rhodamine B) showed a substantial difference, which revealed potentially important applications of the device for characterization of fluorescent materials. For example, the fluorescence quantum yield of a compound can be estimated from the TL and absorption spectra at selected wavelengths over the entire spectrum. This is directly related to the population distributions within the first excited energy level of the molecule at different excitation wavelengths. To demonstrate the applicability of ordinary incoherent light sources in a micro space, Tamaki et al. (2003) proposed a laser defocusing TL detection in a 100 μm microchannel, by utilizing a 250 μm excitation laser beam size in the sample. Excitation with such a large excitation beam size resembles an ILS excitation case. They achieved a LOD of 2×10^{-5} AU for Sunset yellow dye in methanol at a power of 42 mW. They then developed a tunable TL system for microchip analysis (Tamaki et al., 2005). The system utilized a xenon lamp as an excitation source. It could measure the absorption spectrum of a turbid solution without interference from the light scattering background.

We need to note that relatively low LODs (Chartier and Bialkowski, 1997; Tamaki et al., 2003) were achieved in organic solvents (with high dn/dT and low k), which resulted in an enhancement factor of over 10 times higher than in water. Unfortunately, many bioanalytical analyses cannot be performed in organic solvents, which would induce denaturation of biomolecules. This means that in the ILS-based TL system very low sensitivity is expected if the biomolecule or any other analyte is in water. Therefore, it is much desired to improve the sensitivity of the ILS-based TL system. The most commonly used approach is to increase the power or to improve the thermal properties of the sample. But the possible power enhancement of the ILS is very much limited. For example, a maximum power of $\sim$10 mW for a 10 nm bandwidth can be obtained for a xenon lamp between 250 and 1100 nm (Tunable Illuminator, OBB Corp.) after a grating. On the other hand, the thermal properties of aqueous sample solution can also be improved just to a certain limit, which is governed by the achievable mixing ratios and corresponding dilution factors. Therefore, it seems very difficult to improve the sensitivity just from the viewpoint of the enhancement factor. As an alternative, we recently developed an ILS-excited TL system based on a three-layer sample system, as shown in Figure 10. Due to thermal diffusion from the sample layer to the top/bottom layers in a modulation cycle, two additional TL elements will be generated. If the dn/dTs of the top/bottom layers have the same sign as that of the sample layer, namely, all dn/dTs of the three layers are positive or negative, these two additional TL elements will contribute additively to the total TL signal. For a short sample length such as 100 μm, sensitivity enhancement over 10 times can be achieved at 5 Hz if materials with favorable thermal properties are used (Liu et al., 2012). Experimentally, octane was used as the material of the top/bottom layers, and an ILS beam (from 350 to 620 nm) with power of 2.83 mW was used as the excitation source. Compared to the case in a standard 100 μm cell, sensitivity enhancements of 4.7 and 8.5 times were obtained for the two- and three-layer systems, respectively (Liu and Franko, 2012). The LOD for 100 μm ferroin solution was calculated to be 1.3×10^{-6} M (1.5×10^{-4} AU) without signal-enhancement layers or 1.95×10^{-7} M (2.2×10^{-5} AU) with signal-enhancement layers. If the sample is in organic solution, the LOD could go down to $\sim 10^{-6}$ AU even without signal-enhancement layers.

Though a relatively low LOD was obtained for a three-layer sample system in the ILS-excited TL system, several disadvantages limited the application of this system to routine chemical analysis in microchips: (1) low temporal resolution ($\sim$ s) at low modulation frequencies, which will disable the analysis of a flowing sample; (2) large pump/probe beam size (above 200 μm) in the sample plane, which is not compatible with the microchannel; and (3) inconvenience of adding additional layers above or below a flowing sample in the microchannel. Therefore, a practical TLS setup with high sensitivity, high temporal resolution, good compatibility with

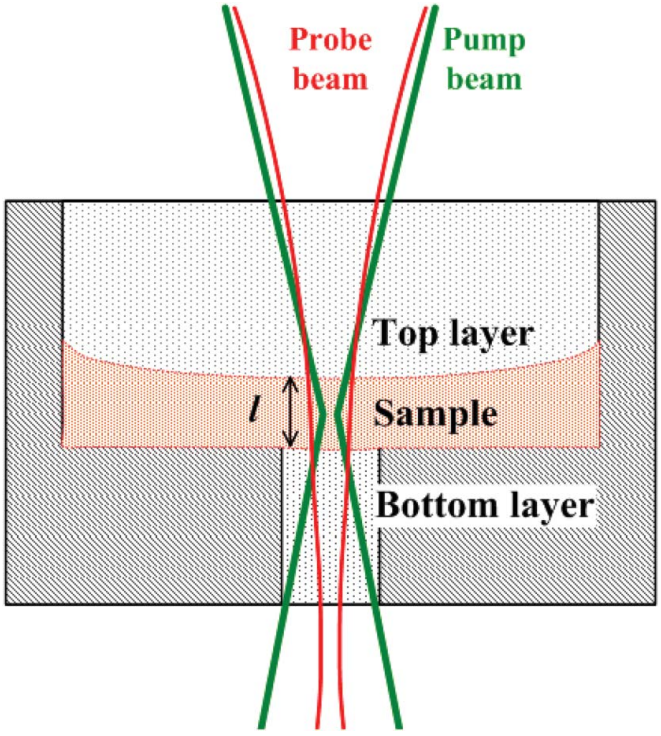

FIG. 10. Schematic graph of the optical configuration of an ILS-excited TL system in a three-layer sample well.

TABLE 1
Applications of different types of TLS for analysis of compounds in the fields of analytical/synthetic chemistry and biochemistry

TL	Sample; Method; Channel size; Flow rate or flow velocity	λ_e/P; f; t_c	Performance (LOD, analysis time, etc.)	Reference(s)
Collinear TLM	SY (in water); 150 × 100 μm	A 488/100	85 ymol in detection volume of 1.3 fL	Sato et al., 1999
	Ferroin and SY; 250 × 100 μm	A 488/40	10 nM of ferroin and 4 nM of SY	Proskurnin et al., 2003
	SY and NiP by *two miniaturized TLMs* (using optical fibers, SELFOC microlenses); quartz cell: 100 μm	DS 532/3.4; LD 658/2.2	1st system: 37 nM SY (1.7×10^{-6} AU); 2nd system: 7.7 nM NiP (3.4×10^{-6} AU).	Tokeshi et al., 2005
	Catecholamine (epinephrine, etc.); 250 × 100 μm	A 488 /570	0.2∼1.2 μg/mL; reaction time: 15 s	Sorouraddin et al., 2001
	Xylenecyanol solution; 250 × 50 μm	LD 635/4.2	30 nM (∼100 times lower than UV-vis)	Mawatari et al., 2005
	Xylene cyanol solution by *reflective TL device*; 1 mm × 50 μm	LD 635/30	60 nM (9.4×10^{-6} AU)	Mawatari et al., 2006
	O-toluidine acidic solution by *EC-TLM*; 160 × 28 μm	A 488 nm	1 μM, 100 times lower than current detection	Kim et al., 2003, 2005
	L-ascorbic acid (AA) and dehydroascorbic acid; 250 × 100 μm	A 514.5/200	0.1 μM	Sorouraddin et al., 2000
	Pb(II) octaethylporphyrin in benzene; 150 × 100 μm	A 488/2; 4 s	0.4 molecule (time average); temperature rise for single molecule: 3.1 μK,	Tokeshi et al., 1999; Tokeshi et al., 2001b
	Fe(II) ion-pair (extracted to chloroform); 250 × 100 μm	A 514.5/200	7.7–180 zmol in 8.6 fL; extraction: 45 s (1 order shorter than ordinary extraction)	Tokeshi et al., 2000
	Co(II) (extracted to m-xylene) wet analysis in multiphase flow network; 140 × 20 μm; Q = 0.2 μL/min	A 488/200	18 nM; analysis time: 50 s (2–3 h in conventional mode)	Tokeshi et al., 2002
	Multi-ion (K^+, Na^+) sensing by intermittently pumping ionophores to organic/aqueous system; 150 × 60 μm	A 514.5/200	$\sim 10^{-4}$ M	Hisamoto et al., 2001b
	Molecular transport (Methyl red) in three-layer flow system (0.1 N hydrochloric acid/cyclohexane/ hydrochloric acid); 192 × 22 μm; Q = 0.3 μL/min for each layer	A 514.5 and 488 nm	Complete equilibration in ∼ seconds (∼ 10 min in conventional method). Molecular transport was in agreement with theory.	Surmeian et al., 2002

Carbaryl pesticide (to toluene) in *micro-multiphase laminar flows*; 226 × 90 μm (deep part) and 185 × 12 μm (shallow part)	Y 532/50	70 nM; analysis time: 8 min.	Smirnova et al., 2006
Carbamate pesticides (carbaryl, carbofuran, etc.) (to 1-butanol); 248 × 94 μm (deep part) and 127 × 23 μm (shallow part)	Y 532/50	10∼30 nM (carbaryl, carbofuran) and 100 nM (bendiocarb); analysis time: 10 min	Smirnova et al., 2007
Ammonia and HRP in *single and dual polymer membranes* prepared by an interfacial polycondensation reaction; 240 × 115 μm (deep part) and 210 × 40 μm (shallow part)	A 514.5/200	Permeation of ammonia through membrane and transformation of chemicals by HRP were observed	Hisamoto et al., 2003
Serum proteins adsorbed to a hemodialysis membrane (stained with colloidal gold); glass slide	A 514.5 nm	Human serum proteins adsorbed: 13 ng per cross section of the membrane.	Kimura et al., 1999
S-IgA (on polystyrene bead) (reacted with gold conjugated with anti-s-IgA antibody) by *immunosorbent assay*; 200 × 100 μm	A 514.5/200	< 1 μg/mL; reaction time: 10 min (15 h in conventional microtiter plate well)	Sato et al., 2000
Carcinoembryonic antigen (reacted with anti-CEA and gold conjugated 2nd antibody) by *sandwich immunoassay*	Y 532/76	0.03 ng/mL and 35 min of analysis time (10 times higher and 45 h in conventional assay)	Sato et al., 2001
Interferon-γ by *microchip-based ELISA*; 200 × 90 μm	Y 532/76	0.1 ng/mL (6 pM); analysis time: 35 min	Sato et al., 2004
BNP (heart failure marker peptide) and NiP by *semiautomatic ELISA on a 32-channel microchip*; 210 × 100 μm	405 nm	Assay time: 20 min (20 h in conventional method); high throughput of 32 ELISA tests	Sato et al., 2003b
Five anthraquinone dyes (in water) by *HPLC-TLM*; sample injection volume: 20 μL; flow cell: ∼ 1 mm × 200 μm	488/28; 1.4 kHz	∼sub-nM (∼140 times better than UV-vis and ∼5 times better than CRDS); 3.5×10^{-8} AU	Li et al., 2007
Adenine aqueous solutions by *UV-TLM* on microchip 100 × 45 μm; fluorene and pyrene by *LC-UV-TLM* in capillary (50 μm)	266/4.3	Adenine 25 nM; fluorene 280 nM; pyrene 520 nM (over 100 times better than UV-vis)	Hiki et al., 2006
Azo dye (preconcentration by sweeping) on an interface chip (IFChip) by *CE-TLM*; capillary (50 μm); channel: 100 × 40 μm	DPSS 488/20; 990 Hz	360 nM; 1.8 pM (sweeping); 10-fold better reproducibility on IFChip than on capillary	Kitagawa et al., 2006
DABSYL-derivatized amino acids (glycine, alanine, etc.) by *CE-TLM on an interface chip* (IFChip); 100 × 40 μm	A 488/200	Pure water: 2.8×10^{-7} AU; amino acids: 24 nM (100 times lower than UV-vis)	Proskurnin et al., 2005a

(continued on next page)

TABLE 1
Applications of different types of TLS for analysis of compounds in the fields of analytical/synthetic chemistry and biochemistry *(continued)*

TL	Sample; Method; Channel size; Flow rate or flow velocity	λ_e/P; f; t_c	Performance (LOD, analysis time, etc.)	Reference(s)
	DNA fragments by *miniaturized ultrathin slab gel electrophoresis*; 25 mm long and 80 μm thick-resolving gel	A 488/4	Theoretical plates: 22000; migration distance: 1/10 of conventional assay	Zheng et al., 1999b
	Polystyrene nanoparticle (130 nm) aqueous solution; 1 × 1 μm; $v_x = 670$ μm/s.	266/4.3; 2.7 kHz; 1 ms	Detection efficiency: 100%	Seta et al., 2009
	80 nm polystyrene particles (containing dye molecules) and 10 nm Ag particles (in water); 150 × 100 μm	A 488/2; 4 kHz; 10 ms	Pulsed signals were clearly distinguished and signal-to-noise ratio was as large as 5	Mawatari et al., 1998
	Detection (counting) and fixation of single and multiple 50 nm gold nanoparticles on the wall of microchannel; 250 × 100 μm	532/20; 1 ms	Fixation on lower wall was attributed to absorption-based optical force	Mawatari et al., 2006
	Molecule detection in a single biological cell (mouse hybridoma); culture medium with cells in glass slide	A 488/20; 20 Hz	37.8 amol/cell	Harada et al., 1999
	In situ imaging of nonfluorescent compounds in a yeast cell; cell was located in quartz slide	TS 261 nm; < 1 mW	Features of 4–8 μm were seen, corresponding to the size of yeast cells.	Harada et al., 2007
	Intercellular messenger (arachidonate) released by stimulating nerve cells; detection channel: 250 × 100 μm	A 244/50	13 μM; cell consumption: 10^3 (1% of conventional method).	Sato et al., 2006
	Monitoring cytochrome *c* (released from mitochondria) in a cell; culture flask: 1 × 10 × 0.1 mm; channel: 250 × 100 μm	YAG 532/100	Cytochrome *c* detected with this system was estimated to be ~10 zmol	Tamaki et al., 2002
	Nitric oxide released from cells in a *microchip-based bioassay system* (culture, heat control, reaction, etc.); 200 × 100 μm	YAG 532/50	LOD: 70 nM and 4 h of assay time (1 μM and 24 h in conventional method)	Goto et al., 2005
	Alkaline phosphatase (ALP) (enzyme marker of osteoblast maturation and osteogenesis); 200 × 100 μm	HN 633 nm	ALP activity: enhanced 10 times compared with the static condition in 48 well dishes.	Jang et al., 2008
	Photothermal temperature control of enzyme reaction by a diode laser (635 nm, 10 mW, irradiation for 5 s); 250 × 100 μm	A 514.5/200	5 μM of reacted H_2O_2	Tanaka et al., 2000
	Photothermal temperature control of enzyme reaction by a diode laser (1472 nm, 150 mW); 250 × 100 μm	A 514.5/200	Fast heating and cooling at 67 and 53°C/s; reaction: controlled with 0.6 s resolution	Slyadnev et al., 2001

	Sensitivity enhancement by light-induced precipitation of analyte (4-aminoazobenzene). Collinear TLS (#1): cell with pathlength of 1 cm; crossed-beam TLS (#2): capillary (75 μm)	#1: 488/170; 4 Hz. #2: HC 325/50; 95 Hz	Collinear TLS: a threefold decrease in LOD to 7 μM; crossed-beam TLS: 3 μM in quartz capillaries	Nedosekin et al., 2009
Crossed beam TLS	Derivatized amino acids by *CE fiber modified TLS*; fused silica capillary: 50 μm I.D.	A 458/150; 80 Hz	Glycine 180 nM.	Seidel and Faubel, 1998
	Amino acids (aqueous solution) by *CE-UV-TLS*; rectangular (100 μm wide) or circular (50 μm I.D.) fused silica capillaries; the probe beam crosses the excitation beam at an angle of 20°	Y 266 nm (20 μJ); 50 Hz	7 μM (tyrosine), 2.5 μM (tryptophan), 33 μM (cysterine), corresponding to 0.35, 0.125, and 1.65 fmol in a 140 pL detection volume	Yu et al., 2009
	2-, 3-, and 4-nitrophenols in 70% v/v acetonitrile separation buffers by *CE-TLS*; capillary: 75 μm I.D.	HC 325/50; 95 Hz	1 μM, 1 μM, and 0.3 μM for 2-, 3-, and 4-nitrophenols	Bendrysheva et al., 2006
	11 nitroaromatic compounds by *MEKC-TLS*; fused-silica capillary: 75 μm I.D.; flow rate: 0.4 mL/min	A 257/120; 85 Hz	0.1∼1 μg/mL (30-fold improvement in comparison with UV-vis)	Ragozina et al., 2002
	Non-labeled amino acids in a square capillary cell (100 μm) by *micro-HPLC-UV-TLS*; flow rate: 10 μL/min	TS 214/3.7; 0.3 s	0.2 to 2.6 μM for 3 amino acids; 8.1 to 120 amol in 44 fL of detection volume	Katae et al., 2010
	1-heptane-, 1-pentane-, 1-butane-, 1-propane-sulfonic and acetic acid (MY 7 as probe ion) by *indirect TLS*; capillary 75 μm.	HC 325/30; 95 Hz	$n \times 10^{-7}$ M	Nedosekin et al., 2007
	TL micro-flow velocimeter (excitation beam is tilted by 30°): v_x measured from the transfer time of TL between two points.	LD 1480/5; 127∼927 Hz	Dynamic range of 25–300 μL/min was measured in a microchannel	Kikutani et al., 2008
CD-TLM	Optically active tris(ethylenediamine)cobalt(III) [Co $(en)_3]^{3+}I_3$- aqueous solutions; quartz cell with a path length of 100 μm	Y 532/100	6.3×10^{-5} M (1.9×10^{-7} abs) (250 times lower than in CD spectrophotometer)	Yamauchi et al., 2006a
	Aqueous solutions of optically active camphorsulfonic acids (CSA) by *UV-CD-TLM*; 250 × 100 μm; v_x = 10 mm/s	Y 266/25	$\sim 8 \times 10^{-4}$ M ($\Delta A = 5 \times 10^{-6}$ Abs) (10 times lower than in CD spectrometer)	Mawatari et al., 2008

(continued on next page)

TABLE 1
Applications of different types of TLS for analysis of compounds in the fields of analytical/synthetic chemistry and biochemistry *(continued)*

TL	Sample; Method; Channel size; Flow rate or flow velocity	λ_e/P; f; t_c	Performance (LOD, analysis time, etc.)	Reference(s)
PM	An array of gold nanorods with nominal sizes 120 × 60 nm and thickness 30 nm on a BK7 glass coverslip	HN632.8 nm; 47 and 94 kHz	Imaging of NP orientation and dichroism (degree of anisotropy)	Zhang et al., 2011
DIC-TLM	Counting of individual gold nanoparticles (5 nm); 500 × 100 μm	A 488 nm	Background: reduced to 1/100; S/B: improved by 1 order of magnitude.	Shimizu et al., 2009
	Aqueous solution of SY in an extended nanochannel; 21 μm × 500 nm	A 488/40; 2.0 kHz	2.4 μM (corresponding to 390 molecules in detection volume of 0.25 fL)	Shimizu et al., 2010
	SY and methyl orange in a mobile phase (water + 20% ACN) by *.extended nanochromatography-DIC-TLM*; 1.3 μm × 500 nm	A 488/27; 2.0 kHz	~10 μM (corresponding to ~1000 molecules in detection volume of 0.25 fL)	Shimizu et al., 2011

A: Ar+ laser; BNP: brain natriuretic peptide; CRDS: cavity ring-down spectroscopy; DABSYL: 4-dimethylaminoazobenzene-4′-sulfonyl; DPSS: diode-pumped solid-state laser; EC-TLM: electrochemical TLM; HC: He-Cd; HN: He-Ne; HRP: horseradish peroxidase; LD: laser diode; MY: mordant yellow 7; NiP: nickel(II) phthalocyaninetetrasulfonic acid tetrasodium salt; PM: polarization modulation TLM; SY: sunset yellow; TS: Ti:sapphire; Y: YAG laser.

The size of microchannels in the second column is given as "width × depth." The wavelength and power of the pump beam in the third column are given as "λ_e (nm)/P (mW)" if both of them are available. For the modulation frequency (f) of the pump beam and the time constant (t_c) of the lock-in amplifier in the third column, only those different from the parameters ($f = \sim 1$ kHz, $t_c = 1$ s) are given.

microfluidics and lab-on-chip chemistry, and good specificity is still the goal of the development of the TLS technique.

Applications

In combination with different techniques, such as continuous-flow microanalysis, microchromatography, and separation techniques, TLM or TL systems have been utilized in various applications in the fields of analytical chemistry (immunoassays, CE, extraction processes, and enzymatic catalysis), synthetic chemistry (study of transfer of substances across a boundary surface, study of impacts of different factors on chemical reactions and polymerization in microchips), and biochemistry (detection of compounds within a cell). Most of these applications have been described in original as well as review articles (Dudkoa et al., 2012; Franko and Tran, 2011; Ghaleb and Georges, 2004; Kitamori et al., 2004; Tokeshi et al., 2003). Here, instead of repeated descriptions of these applications, we summarize them in Table 1, in which they are grouped into five categories of TLS: collinear TLM, crossed-beam TLS, CD-TLM, PM-TLM, and DIC-TLM. Though both CD-TLM and PM-TLM are actually collinear TLMs, in the table they are listed separately from the general collinear TLMs since their excitation modes are different: CD-TLM uses left- and right-circularly polarized light beams for alternate excitations, PM-TLM employs a linearly polarized beam (whose polarization angle is sinusoidally modulated) for excitation, while the general collinear TLM uses an intensity-modulated beam for excitation. Basic characteristics of used microchips, excitation lasers, and LODs are reported for each analyte.

From the table we can see that most of the applications are based on collinear TLMs, by which different analyte molecules (dyes; amino acids; amines; proteins; antigens, such as secretory immunoglobulin A (s-IgA), human leukocyte antigen (HLA), and carcinoembryonic antigen; enzymes; metal ions; pesticides; pharmaceuticals, such as amphetamines, sedatives, and antibiotics; and nanoparticles, among others) in chemical/physical (reaction, immunoassay, separation, extraction) or biological processes (stimulation, secretion) in one-phase or two-/three-phase systems (separated by two immiscible [aqueous/organic] solvents, polymer membranes, or biological membranes [cell membrane]) were detected. In addition, temperature control of chemical reactions and light-induced precipitation for sensitivity enhancement were investigated in collinear TLM as well. Crossed-beam TL systems have been combined with CE, MEKC, and HPLC for detection of amino acids, sulfonic/acetic acids, nitrophenols, and nitroaromatic compounds, and one application of measuring flow velocity in a microchannel was also reported. CD-TLM has been used for detection of chiral compounds such as $[Co(en)_3]^{3+}I_3$- and camphorsulfonic acids in visible and UV regions, respectively. As newly emerging techniques, PM-TLM was used for imaging the orientation of nonspherical nanoparticles, and DIC-TLM was employed for nanoparticle counting or analyte detection in extended nanochannels.

CONCLUSIONS AND PROSPECTS

Recent developments of TLS and its applications for chemical analysis in micro space and particularly in microfluidic devices are mainly focused on (1) detection sensitivity enhancement (by optimizing optical parameters, such as pump power/power density, modulation frequency, mode-mismatching between pump and probe beams, and pump-to-probe beam offset for flowing samples and sample parameters, such as flow velocity, and solvents), (2) noise reduction (by choosing appropriate modulation frequency and pinhole-to-beam size ratio at the detection plane and flow velocity, and/or by employing proper detection mode when necessary, such as differential detection), (3) specificity improvement (by employing available laser lines from UV to IR, and incoherent light sources), and (4) system miniaturization (by incorporating micro optical and mechanical components). Although TLM has advanced considerably over 10 years of development, the instrumentation still doesn't reach the required maturity, and the corresponding applications are limited to only certain compounds or groups of compounds. Therefore, to develop TLS into a regular technique for routine chemical analysis, much more work is needed for successful implementation for analysis of real samples. Two directions for the development of TLS can be foreseen:

1. To develop more automated laser-excited TLS (especially TLM) instruments and expand their applications for detecting various compounds or monitoring more complicated physical, chemical, and biochemical processes. For example, TLM can be used for analysis of new emerging pollutants in the environment (such as plasticizers in foodstuffs), important biomarkers and substances in human serum samples (such as neutrophil gelatinase-associated lipocalin), and other real samples with complex matrices in a physically or chemically modified microchannel on a chip integrated with different micro unit operations (Kikutani et al., 2004; Mawatari et al., 2011a; Yamasaki et al., 2009). On the other hand, TLM could be used for studying molecular diffusion, reaction kinetics, and organ modeling (Tanaka et al., 2007) in single- or multiple-phase microfluidic systems, and even in/around droplets in a microchannel. It is worth noting that performing chemical analysis in droplets by TLM is quite promising since droplet microfluidics enables high-throughput screening in particularly small-volume compartments, in which sensitivity could be enhanced by increasing the effective concentration of rare species and assay time could be further decreased (Guo et al., 2012). To make TLM compatible with the curved surface of the droplets, both the optical configuration of TLM system should be improved and the

shape of the droplets properly manipulated. In addition, applying TLM to nanoscale space for detecting nanoparticles or investigating some new phenomena in extended nanochannels (Kitamori, 2007; Mawatari et al., 2010), such as monitoring single-cell proteomics and metabolomics by integrating immunoassay into extended nano space (Sato et al., 2008), is also very interesting.

2. To construct practical TLS instruments characterized by portability for in situ applications, low cost, and possibility of performing parallel operations and for integration with microchips. This requires that the TLS should not have just high sensitivity and low detection limits in various solvents, but also a compact size and as good specificity as conventional transmission techniques. To achieve this, developing a practical incoherent light source (especially LED; Kuo et al., 2004)-excited TLS setup is a feasible way. This work is already in progress in our lab.

To achieve more detailed and richer information about an analyte (Baker et al., 2009), TLS could also be combined with other detection techniques, such as fluorescence detection, electrochemical analysis, MS, surface-enhanced Raman scattering (qualitatively identifying analytes; Connaster et al., 2008), and surface plasmon resonance (studying binding interactions in biological assays without use of labels; Luo et al., 2008).

REFERENCES

Baker, C. A.; Duong, C. T.; Grimley, A.; Roper, M. G. Recent Advances in Microfluidic Detection Systems. *Bioanalysis* **2009**, *1*, 967–975.

Baptista, M.; Tran, C. D. Near-Infrared Thermal Lens Spectrometer Based on an Erbium-Doped Fiber Amplifier and an Acousto-Optic Tunable Filter, and Its Application in the Determination of Nucleotides. *Appl. Opt.* **1997**, *36*, 7059–7065.

Bendrysheva, S. N.; Proskurnin, M. A.; Pyell, U.; Faubel, W. Sensitivity Improvement in Capillary Electrophoresis Using Organo-Aqueous Separation Buffers and Thermal Lens Detection. *Anal. Bioanal. Chem.* **2006**, *385*, 1492–1503.

Bialkowski, S. E. *Photothermal Spectroscopy Methods for Chemical Analysis*; John Whiley & Sons: New York, 1996.

Bialkowski, S. E.; Chartier, A. Photothermal Spectrometry in Small Liquid Channels. *Anal. Sci.* **2001**, *17*(Suppl.), i99–i101.

Bicanic, D.; Franko, M.; Gibkes, J.; Gerkema, E.; Favier, J. P.; Jalink, H. Applications of Photoacoustic and Photothermal Non-contact Methods in the Selected Areas of Environmental and Agricultural Sciences. In *Progress in Photothermal and Photoacoustic Science and Technology, Vol. 3, Life and Earth Sciences*; Mandelis, A., Ed.; SPIE-Optical Engineering Press: Bellingham, Wash., 1996; p 131.

Bicanic, D.; Močnik, G.; Franko, M.; Niederländer, H. A. G.; Bovenkamp, P. V.; Cozijnsen, J.; Klift, E. V. Separation and Direct Detection of Long Chain Fatty Acids and Their Methylesters by the Nonaqueous Reversed Phase HPLC and Silver Ion Chromatography, Combined with CO Laser Pumped Thermal Lens Spectrometry. *Instrum. Sci. Technol.* **2006**, *34*, 129–150.

Bindhu, C. V.; Harilal, S. S.; Nampoori, V. P. N.; Vallabhan, C. P. G. Investigation of Nonlinear Absorption and Aggregation in Aqueous Solutions of Rhodamine B Using Thermal Lens Technique. *Pramana* **1999**, *52*, 435–442.

Boškin, A. The Application of High Sensitivity Laser Methods for Detection of Organophosphorus Pesticides and Cholinesterase Activity, Ph.D. Thesis, University of Nova Gorica, Nova Gorica, Slovenia, 2008.

Boškin, A.; Tran, C. D.; Franko, M. Oxidation of Organophosphorus Pesticides with Chloroperoxidase Enzyme in the Presence of an Ionic Liquid as Co-solvent. *Environ. Chem. Lett.* **2009**, *7*, 267–270.

Cabrera, H.; Sira, E.; Rahn, K.; García-Sucre, M. A Thermal Lens Model Including the Soret Effect. *Appl. Phys. Lett.* **2009**, *94*, 051103.

Chanlon, S.; Georges, J. Pulsed-Laser Mode-Mismatched Crossed-Beam Thermal Lens Spectrometry within a Small Capillary Tube: Effect of Flow Rate and Beam Offset on the Photothermal Signal. *Spectrochim. Acta A* **2002**, *58*, 1607–1613.

Chartier, A.; Bialkowski, S. E. Photothermal Lens Spectrometry of Homogeneous Fluids with Incoherent White-Light Excitation Using a Cylindrical Sample Cell. *Opt. Eng.* **1997**, *36*, 303–311.

Chen, I. H.; Chu, S. W.; Sun, C. K.; Cheng, P. C.; Lin, B. L. Wavelength Dependent Damage in Biological Multi-photon Confocal Microscopy: A Micro-spectroscopic Comparison between Femtosecond Ti:sapphire and Cr:forsterite Laser Sources. *Opt. Quantum Electron.* **2002**, *34*, 1251–1266.

Connaster, R. M.; Cochran, M.; Harrison, R. J.; Sepaniak, M. J. Analytical Optimization of Nanocomposite Surface-Enhanced Raman Spectroscopy/Scattering Detection in Microfluidic Separation Devices. *Electrophoresis* **2008**, *29*, 1441–1450.

Crevillén, A. G.; Avila, M.; Pumera, M.; Gonzalez, M. C.; Escarpa, A. Food Analysis on Microfluidic Devices Using Ultrasensitive Carbon Nanotubes Detectors. *Anal. Chem.* **2007**, *79*, 7408–7415.

Divjak, B.; Franko, M.; Novič, M. Determination of Iron Complex Matrices by Ion Chromatography with UV-Vis, Thermal Lens and Amperometric Detection Using Post-Column Reagents. *J. Chromatogr. A* **1998**, *829*, 167–174.

Dovichi, N. J. Thermo-optical Spectrophotometries in Analytical Chemistry. *Crit. Rev. Anal. Chem.* **1987**, *17*, 357–423.

Dovichi, N. J.; Harris, J. M. Thermal Lens Calorimetry for Flowing Samples. *Anal. Chem.* **1981**, *53*, 689–692.

Dudkoa, V. S.; Smirnova, A. P.; Proskurnin, M. A.; Hibara, A.; Kitamori, T.;. Thermal Lens Detection in Microfluidic Chips. *Russ. J. Gen. Chem.* **2012**, *82*, 2146–2153.

Erskine, S. R.; Bobbitt, D. R. Theoretical and Experimental Investigation of the Relationship between Aperture Dimension and Signal-to-Noise Optimization in Thermal Lens Spectroscopy. *Appl. Spectrosc.* **1988**, *42*, 331–335.

Erskine, S. R.; Bobbitt, D. R. Obliquely Crossed, Differential Thermal Lens Measurements under Conditions of High Background Absorbance. *Appl. Spectrosc.* **1989**, *43*, 668–674.

Fang, H. C.; Swoford, R. L. The Thermal Lens in Absorption Spectroscopy. In *Ultrasensitive Laser Spectroscopy*; Kliger, D. S., Ed.; Academic Press: New York, 1983; p 175.

Faubel, W.; Heissler, S.; Pyell, U.; Ragozina, N. Photothermal Trace Detection in Capillary Electrophoresis for Biomedical

Diagnostics and Toxic Materials. *Rev. Sci. Instrum.* **2003**, *74*, 491–494.

Franko, M. Thermal Lens Spectrometric Detection in Flow Injection Analysis and Separation Techniques. *Appl. Spectrosc. Rev.* **2008**, *43*, 358–388.

Franko, M. Bioanalytical Applications of Thermal Lens Spectrometry. In *Thermal Wave Physics and Related Photothermal Techniques: Basic Principles and Recent Developments*; Moares, E. M., Ed.; Transworld Research Network: Kerala, India, 2009; p 309.

Franko, M.; Bicanic, D. Differential Thermal Lens Spectroscopy in the Infrared. *Israel J. Chem.* **1998**, *38*, 175–179.

Franko, M.; Tran, C. D. Water as a Unique Medium for Thermal Lens Measurements. *Anal. Chem.* **1989**, *61*, 1660–1666.

Franko, M.; Tran, C. D. Thermal Lens Technique for Sensitive Kinetic Determinations of Fast Chemical Reactions. Part I. Theory. *Rev. Sci. Instrum.* **1991a**, *62*, 2430–2437.

Franko, M.; Tran, C. D. Thermal Lens Technique for Sensitive Kinetic Determinations of Fast Chemical Reactions. Part II. Experiment. *Rev. Sci. Instrum.* **1991b**, *62*, 2438–2442.

Franko, M.; Tran, C. D. Analytical Thermal Lens Instrumentation. *Rev. Sci. Instrum.* **1996**, *67*, 1–18.

Franko, M.; Tran, C. D. Thermal Lens Spectroscopy. In *Encyclopedia of Analytical Chemistry*; Meyers, R. A., Ed.; Wiley: Chichester, 2011; p 1249.

Georges, J. Advantages and Limitations of Thermal Lens Spectrometry over Conventional Spectrophotometry for Absorbance Measurements. *Talanta* **1999**, *48*, 501–509.

Georges, J. Matrix Effects in Thermal Lens Spectrometry: Influence of Salts, Surfactants, Polymers and Solvent Mixtures. *Spectrochim. Acta A* **2008**, *69*, 1063–1072.

Georges, J.; Arnaud, N.; Parise, L. Limitations Arising from Optical Saturation in Fluorescence and Thermal Lens Spectrometries Using Pulsed Laser Excitation: Application to the Determination of the Fluorescence Quantum Yield of Rhodamine 6G. *Appl. Spectrosc.* **1996**, *50*, 1505–1511.

Ghaleb, K. A.; Georges, J. Photothermal Spectrometry for Detection in Miniaturized Systems: Relevant Features, Strategies and Recent Applications. *Spectrochim. Acta A* **2004**, *60*, 2793–2801.

Goto, M.; Sato, K.; Murakami, A.; Tokeshi, M.; Kitamori, T. Development of a Microchip-Based Bioassay System Using Cultured Cells. *Anal. Chem.* **2005**, *77*, 2125–2131.

Grishko, V. I.; Tran, C. D.; Duley, W. W. Enhancement of the Thermal Lens Signal Induced by Sample Matrix Absorption of the Probe Laser Beam. *Appl. Opt.* **2002**, *41*, 5814–5822.

Guo, M. T.; Rotem, A.; Heyman, J. A.; Weitz, D. A. Droplet Microfluidics for High-Throughput Biological Assays. *Lab Chip* **2012**, *12*, 2146–2155.

Gupta, R. Theory of Photothermal Effect in Fluids. In *Photothermal Investigations of Solids and Fluids*; Sell, J. A., Ed.; Academic Press: New York, 1988; p 81.

Guzsvány, V.; Madžgalj, A.; Trebše, P.; Gaál, F.; Franko, M. Determination of Selected Neonicotinoid Insecticides by Liquid Chromatography with Thermal Lens Spectrometric Detection. *Environ. Chem. Lett.* **2007**, *5*, 203–208.

Harada, M.; Iwamoto, K.; Kitamori, T.; Sawada, T. Photothermal Microscopy with Excitation and Probe Beams Coaxial under the Microscope and Its Application to Microparticle Analysis. *Anal. Chem.* **1993**, *65*, 2938–2940.

Harada, M.; Shibata, M.; Kitamori, T.; Sawada, T. Sub-Attomole Molecule Detection in a Single Biological Cell In-Vitro by Thermal Lens Microscopy. *Anal. Sci.* **1999**, *15*, 647–650.

Harata, A. Enhanced Photothermal Spectroscopy for Observing Chemical Reactions in Biological Cells. In *Handai Nanophotonics*; Masuhara, H.; Kawata S.; Tokunaga F., Eds.; Elsevier: Amsterdam, 2007; Vol. 3; p 73.

Harata, A.; Yamaguchi, N. Photothermal Lensing Signal Enhancement by the Transient Absorption of Photoexcited States in Liquid Solutions. *Anal. Sci.* **2000**, *16*, 743–749.

Harata, A.; Fukushima, K.; Harano, Y. Magnification in Excess of 100-Times of the Microscopic Photothermal Lensing Signal from Solute Molecules by Two-Color Excitation with Continuous-Wave Lasers. *Anal. Sci.* **2002**, *18*, 1367–1373.

Harata, A.; Matuda, T.; Hirashima, S. Ultraviolet-Laser Excitation Microscopic Photothermal Lens Imaging for Observing Biological Cells. *Jpn. J. Appl. Phys.* **2007**, *46*, 4561–4563.

Harris, J. Thermal Lens Effect. In *Analytical Applications of Lasers*; Piepmeier, E. H., Ed.; Wiley Interscience: New York, 1986; p 451.

Hiki, S.; Mawatari, K.; Hibara, A.; Tokeshi, M.; Kitamori, T. UV Excitation Thermal Lens Microscope for Sensitive and Nonlabeled Detection of Nonfluorescent Molecules. *Anal. Chem.* **2006**, *78*, 2859–2863.

Hisamoto, H.; Horiuchi, T.; Tokeshi, M.; Hibara, A.; Kitamori, T. On-Chip Integration of Neutral Ionophore-Based Ion Pair Extraction Reaction. *Anal. Chem.* **2001a**, *73*, 1382–1386.

Hisamoto, H.; Horiuchi, T.; Uchiyama, K.; Tokeshi, M.; Hibara, A.; Kitamori, T. On-Chip Integration of Sequential Ion Sensing System Based on Intermittent Reagent Pumping and Formation of Two-Layer Flow. *Anal. Chem.* **2001b**, *73*, 5551–5556.

Hisamoto, H.; Shimizu, Y.; Uchiyama, K.; Tokeshi, M.; Kikutani, Y.; Hibara, A.; Kitamori, T. Chemicofunctional Membrane for Integrated Chemical Processes on a Microchip. *Anal. Chem.* **2003**, *75*, 350–354.

Jang, K.; Sato, K.; Igawa, K.; Chung, U.; Kitamori, T. Development of an Osteoblast-Based 3D Continuous-Perfusion Microfluidic System for Drug Screening. *Anal. Bioanal. Chem.* **2008**, *390*, 825–832.

Kachanov, A. Thermal Lens Spectroscopy for Ultra-Sensitive Absorption Measurement. U.S. Patent Application, US2008/0144007A1, 2008.

Katae, H.; Hirashima, S.; Harata, A. Direct Detection of Gradient-Eluted Non-labeled Amino Acids Using Micro-HPLC with Ultraviolet Thermal Lensing. *J. Phys. Conf. Ser.* **2010**, *214*, 012122.

Kikutani, Y.; Hisamoto, H.; Tokeshi, M.; Kitamori, T. Micro Wet Analysis System Using Multi-phase Laminar Flows in Three-Dimensional Microchannel Network. *Lab Chip* **2004**, *4*, 328–332.

Kikutani, Y.; Ueno, M.; Hisamoto, H.; Tokeshi, M.; Kitamori, T. Continuous-Flow Chemical Processing in Three-Dimensional Microchannel Network for On-Chip Integration of Multiple Reactions in a Combinatorial Mode. *QSAR Comb. Sci.* **2005**, *24*, 742–757.

Kikutani, Y.; Mawatari, K.; Katayama, K.; Tokeshi, M.; Fukuzawa, T.; Kitaoka, M.; Kitamori, T. Flowing Thermal Lens Micro-flow Velocimeter. *Sens. Actuators B* **2008**, *133*, 91–96.

Kim, H.-B.; Hagino, T.; Sasaki, N.; Kitamori, T. Ultrasensitive Detection of Electrochemical Reactions by Thermal Lens Microscopy for Microchip Chemistry. In *Proceedings of μTAS 2003 Seventh International Conference on Micro Total Analysis*

Systems; Northrup M. A.; Jensen K. F.; Harrison D. J., Eds.; Transducers Research Foundation: Cleveland, 2003; Vol. 1; p 817.

Kim, H.-B.; Hagino, T.; Sasaki, N.; Watanabe, N.; Kitamori, T. Spectroelectrochemical Detection Using Thermal Lens Microscopy with a Glass-Substrate Microelectrode-Microchannel Chip. *J. Electroanal. Chem.* **2005**, *577*, 47–53.

Kimura, H.; Kojima, H.; Mukaida, M.; Kitamori, T.; Sawada, T. Analysis of Serum Proteins Adsorbed to a Hemodialysis Membrane of Hollowfiber Type by Thermal Lens Microscopy. *Anal. Sci.* **1999**, *15*, 1101–1107.

Kitagawa, F.; Tsuneka, T.; Akimoto, Y.; Sueyoshi, K.; Uchiyama, K.; Hattori, A.; Otsuka, K. Toward Million-Fold Sensitivity Enhancement by Sweeping in Capillary Electrophoresis Combined with Thermal Lens Microscopic Detection Using an Interface Chip. *J. Chromatogr. A* **2006**, *1106*, 36–42.

Kitamori, T. Micro and Nano Chemical System on Chip. Paper presented at 14th International Conference on Solid-State Sensors, Actuators and Microsystems, Lyon, France, June 10–14, 2007.

Kitamori, T.; Tokeshi, M.; Hibara, A.; Sato, K. Thermal Lens Microscopy and Microchip Chemistry. *Anal. Chem.* **2004**, *76*, 52A–60A.

Kuo, J. S.; Kuyper, C. L.; Allen, P. B.; Fiorini, G. S.; Chiu, D. T. High-Power Blue/UV Light-Emitting Diodes as Excitation Sources for Sensitive Detection. *Electrophoresis* **2004**, *25*, 3796–3804.

Lazar, I. M.; Grym, J.; Foret, F. Microfabricated Devices: A New Sample Introduction Approach to Mass Spectrometry. *Mass Spectrom. Rev.* **2006**, *25*, 573–594.

Li, B.; Xiong, S.; Zhang, Y. Fresnel Diffraction Model for Mode-Mismatched Thermal Lens with Top-Hat Beam Excitation. *Appl. Phys. B* **2005**, *80*, 527–534.

Li, F.; Kachanov, A. A.; Zare, R. N. Detection of Separated Analytes in Subnanoliter Volumes Using Coaxial Thermal Lensing. *Anal. Chem.* **2007**, *79*, 5264–5271.

Liu, M.; Franko, M. An Incoherent Light Source Excited Thermal Lens Microscope. *Appl. Phys. Lett.* **2012**, *100*, 121110.

Liu, M.; Franko, M. A Flexible Thermal Lens Microscope for Detection in a Microfluidic Chip. *Appl. Phys. Lett.* **2014a**.

Liu, M.; Franko, M. Combined μFIA and TLM Device for Rapid Determination of Hexavalent Chromium. *Anal. Chim. Acta* **2014b**.

Liu, M.; Franko, M. Thermal Lens Spectrometry under Excitation of a Divergent Pump Beam. *Appl. Phys. B* **2013**. Advance online publication. DOI: 10.1007/s00340-013-5601-4.

Liu, M.; Korte, D.; Franko, M. Theoretical Description of Thermal Lens Spectrometry in Micro Space. *J. Appl. Phys.* **2012**, *111*, 033109.

Liu, M.; Novak, U.; Plazl, I.; Franko, M. Optimization of a Thermal Lens Microscope for Detection in a Microfluidic Chip. *Int. J. Thermophys.* **2013**. Advance online publication. DOI: 10.1007/s10765-013-1515-y.

Livak-Dahl, E.; Sinn, I.; Burns, M. Microfluidic Chemical Analysis Systems. *Annu. Rev. Chem. Biomol. Eng.* **2011**, *2*, 325–353.

Luo, Y.; Yu, F.; Zare, R. N. Microfluidic Device for Immunossays Based on Surface Plasmon Resonance Imaging. *Lab Chip* **2008**, *8*, 694–700.

Madžgalj, A.; Baesso, M. L.; Franko, M. Flow Injection–Thermal Lens Spectrometric Determination of Hexavalent Chromium. *Eur. Phys. J. Spec. Topics* **2008**, *153*, 503–506.

Malacarne, L. C.; Astrath, N. G. C.; Medina, A. N.; Herculano, L. S.; Baesso, M. L.; Pedreira, P. R. B.; Shen, J.; Wen, Q.; Michaelian, K. H.; Fairbridge, C. Soret Effect and Photochemical Reaction in Liquids with Laser-Induced Local Heating. *Opt. Express* **2011**, *19*, 4047–4058.

Marcano O. A.; Ojeda, J.; Melikechi, N. Absorption Spectra of Dye Solutions Measured Using a White Light Thermal Lens Spectrophotometer. *Appl. Spectrosc.* **2006**, *60*, 560–563.

Marcano O. A.; Delima, F.; Markushin, Y.; Melikechi, N. Determination of Linear and Nonlinear Absorption of Metallic Colloids Using Photothermal Lens Spectrometry. *J. Opt. Soc. Am. B* **2011**, *28*, 281–287.

Mawatari, K.; Shimoide, K. Reflective Thermal Lens Detection Device. *Lab Chip* **2006**, *6*, 127–130.

Mawatari, K.; Kitamori, T.; Sawada, T. Individual Detection of Single-Nanometer-Sized Particles in Liquid by Photothermal Microscope. *Anal. Chem.* **1998**, *70*, 5037–5041.

Mawatari, K.; Naganuma, Y.; Shimoide, K. Portable Thermal Lens Spectrometer with Focusing System. *Anal. Chem.* **2005**, *77*, 687–692.

Mawatari, K.; Tokeshi, M.; Kitamori, T. Quantitative Detection and Fixation of Single and Multiple Gold Nanoparticles on a Microfluidic Chip by Thermal Lens Microscope. *Anal. Sci.* **2006**, *22*, 781–784.

Mawatari, K.; Kubota, S.; Kitamori, T. Circular Dichroism Thermal Lens Microscope in the UV Wavelength Region (UV-CD-TLM) for Chiral Analysis on a Microchip. *Anal. Bioanal. Chem.* **2008**, *391*, 2521–2526.

Mawatari, K.; Tsukahara, T.; Sugii, Y.; Kitamori, T. Extended-Nano Fluidic Systems for Analytical and Chemical Technologies. *Nanoscale* **2010**, *2*, 1588–1595.

Mawatari, K.; Kazoe, Y.; Aota, A.; Tsukahara, T.; Sato, K.; Kitamori, T. Microflow Systems for Chemical Synthesis and Analysis: Approaches to Full Integration of Chemical Process. *J. Flow Chem.* **2011a**, *1*, 3–12.

Mawatari, K.; Ohashi, T.; Ebata, T.; Tokeshi, M.; Kitamori, T. Thermal Lens Detection Device. *Lab Chip* **2011b**, *11*, 2990–2993.

Nakanishi, K.; Imasaka, T.; Ishibashi, N. Thermal Lens Spectrophotometry of Phosphorus Using a Near-Infrared Semiconductor Laser. *Anal. Chem.* **1985**, *57*, 1219–1223.

Navas, M. J.; Jiménez, A. M. Thermal Lens Spectrometry as Analytical Tool. *Crit. Rev. Anal. Chem.* **2003**, *33*, 77–88.

Nedosekin, D. A.; Bendrysheva, S. N.; Faubel, W.; Proskurnin, M. A.; Pyell, U. Indirect Thermal Lens Detection for Capillary Electrophoresis. *Talanta* **2007**, *71*, 1788–1794.

Nedosekin, D. A.; Faubel, W.; Proskurnin, M. A.; Pyell, U. Sensitivity Enhancement of Thermal-Lens Spectrometry Using Laser-Induced Precipitation. *Anal. Sci.* **2009**, *25*, 611–616.

Nickolaisen, S. L.; Bialkowski, S. E. Pulsed Laser Thermal Lens Spectrophotometry for Flowing Liquid Detection. *Anal. Chem.* **1986**, *58*, 215–220.

Okabare, P. I.; Soper, S. A. High Throughput Single Molecule Detection for Monitoring Biochemical Reactions. *Analyst* **2009**, *134*, 97–106.

Otsuka, K. Chiral Separations Using Avidin as a Chiral Selector and Highly Sensitive Detection Using Thermal Lens Microscopy in Capillary Electrophoresis. *Chromatography* **2007**, *28*, 1–7.

Pedreira, P. R. B.; Hirsch, L. R.; Pereira, J. R. D.; Medina, A. N.; Bento, A. C.; Baesso, M. L.; Rollemberg, M. C.; Franko, M.; Shen,

J. Real-Time Quantitative Investigation of Photochemical Reaction Using Thermal Lens Measurements: Theory and Experiment. *J. Appl. Phys.* **2006**, *100*, 044906.

Plumb, D. M.; Harris, J. M. Absorbance Measurements in Optically Inhomogeneous Samples Using Phase-Conjugate Thermal Lens Spectroscopy. *Appl. Spectrosc.* **1992**, *46*, 1346–1353.

Pogačnik, L.; Franko, M. Optimisation of FIA System for Detection of Organophosphorus and Carbamate Pesticides Based on Cholinesterase Inhibition. *Talanta* **2001**, *54*, 631–641.

Proskurnin, M. A.; Kononets, M. Y. Modern Analytical Thermooptical Spectroscopy. *Russ. Chem. Rev.* **2004**, *73*, 1143–1172.

Proskurnin, M. A.; Volkov, M. E. Mode-Mismatched Dual-Beam Differential Thermal Lensing with Optical Scheme Design Optimized Using Expert Estimation for Analytical Measurements. *Appl. Spectrosc.* **2008**, *62*, 439–449.

Proskurnin, M. A.; Slyadnev, M. N.; Tokeshi, M.; Kitamori, T. Optimisation of Thermal Lens Microscopic Measurements in a Microchip. *Anal. Chim. Acta* **2003**, *480*, 79–95.

Proskurnin, M. A.; Chernysh, V. V.; Filichkina, V. A. Some Metrological Aspects of the Optimization of Thermal-Lens Procedures. *J. Anal. Chem.* **2004**, *59*, 818–827.

Proskurnin, M. A.; Bendrysheva, S. N.; Ragozina, N.; Heissler, S.; Faubel, W.; Pyell, U. Optimization of Instrumental Parameters of a Near-Field Thermal-Lens Detector for Capillary Electrophoresis. *Appl. Spectrosc.* **2005a**, *59*, 1470–1479.

Proskurnin, M. A.; Chernysh, V. V.; Kononets, M. Y.; Pakhomova, S. V. Thermal Lens Spectrometry as a Tool for Determination of Stability Constants of Complex Compounds. *Russ. Chem. Bull. (Int. Ed.)* **2005b**, *54*, 124–134.

Proskurnin, M. A.; Ryndina, E. S.; Tsarkov, D. S.; Shkinev, V. M.; Smirnova, A.; Hibara, A. Comparison of Performance Parameters of Photothermal Procedures in Homogeneous and Heterogeneous Systems. *Anal. Sci.* **2011**, *27*, 381–387.

Qi, M.; Li, X. F.; Stathakis, C.; Dovichi, N. J. Capillary Electrochromatography with Thermo-Optical Absorbance Detection for the Analysis of Phenylthiohydantoin-Amino Acids. *J. Chromatogr. A* **1999**, *853*, 131–140.

Ragozina, N.; Heissler, S.; Faubel, W.; Pyell, U. Near-Field Thermal Lens Detection at 257 nm as an Alternative to Absorption Spectrometric Detection in Combination with Electromigrative Separation Techniques. *Anal. Chem.* **2002**, *74*, 4480–4487.

Ramis-Ramos, G.; Baeza Baeza, J. J.; Simó Alfonso, E. F. A Model for Optical Saturation Thermal Lens Spectrometry. *Anal. Chim. Acta* **1994**, *296*, 107–113.

Sato, K.; Kawanishi, H.; Tokeshi, M.; Kitamori, T.; Sawada, T. Subzeptomole Detection in a Microfabricated Glass Channel by Thermal-Lens Microscopy. *Anal. Sci.* **1999**, *15*, 525–529.

Sato, K.; Tokeshi, M.; Odake, T.; Kimura, H.; Ooi, T.; Nakao, M.; Kitamori, T. Integration of an Immunosorbent Assay System: Analysis of Secretory Human Immunoglobulin A on Polystyrene Beads in a Microchip. *Anal. Chem.* **2000**, *72*, 1144–1147.

Sato, K.; Tokeshi, M.; Kimura, H.; Kitamori, T. Determination of Carcinoembryonic Antigen in Human Sera by Integrated Bead-Bed Immunoassay in a Microchip for Cancer Diagnosis. *Anal. Chem.* **2001**, *73*, 1213–1218.

Sato, K.; Hibara, A.; Tokeshi, M.; Hisamoto, H.; Kitamori, T. Microchip-Based Chemical and Biochemical Analysis Systems. *Adv. Drug Deliv. Rev.* **2003a**, *55*, 379–391.

Sato, K.; Yamanaka, M.; Tokeshi, M.; Morishima, K.; Kitamori, T. Multichannel Micro ELISA System. In *Proceedings of μTAS 2003 Seventh International Conference on Micro Total Analysis Systems*; Northrup M. A.; Jensen K. F.; Harrison D. J., Eds.; Transducers Research Foundation: Cleveland, 2003; Vol. 1; p 781.

Sato, K.; Yamanaka, M.; Hagino, T.; Tokeshi, M.; Kimura, H.; Kitamori, T. Microchip-Based Enzyme-Linked Immunosorbent Assay (MicroELISA) System with Thermal Lens Detection. *Lab Chip* **2004**, *4*, 570–575.

Sato, K.; Egami, A.; Odake, T.; Tokeshi, M.; Aihara, M.; Kitamori, T. Monitoring of Intercellular Messengers Released from Neuron Networks Cultured in a Microchip. *J. Chromatogr. A* **2006**, *1111*, 228–232.

Sato, K.; Mawatari, K.; Kitamori, T. Microchip-Based Cell Analysis and Clinical Diagnosis System. *Lab Chip* **2008**, *8*, 1992–1998.

Seidel, B. S.; Faubel, W. Fiber Optic Modified Thermal Lens Detector System for the Determination of Amino Acids. *J. Chromatogr. A* **1998**, *817*, 223–226.

Seta, N.; Mawatari, K.; Kitamori, T. Individual Nanoparticle Detection in Liquid by Thermal Lens Microscope and Improvement of Detection Efficiency Utilizing 1μm Microfluidic Channel. *Anal. Sci.* **2009**, *25*, 275–278.

Sheldon, S. J.; Knight, L. V.; Thorne, J. M. Laser-Induced Thermal Lens Effect: A New Theoretical Model. *Appl. Opt.* **1982**, *21*, 1663–1669.

Shimizu, H.; Mawatari, K.; Kitamori, T. Development of a Differential Interference Contrast Thermal Lens Microscope for Sensitive Individual Nanoparticle Detection in Liquid. *Anal. Chem.* **2009**, *81*, 9802–9806.

Shimizu, H.; Mawatari, K.; Kitamori, T. Sensitive Determination of Concentration of Nonfluorescent Species in an Extended-Nanochannel by Differential Interference Contrast Thermal Lens Microscope. *Anal. Chem.* **2010**, *82*, 7479–7484.

Shimizu, H.; Mawatari, K.; Kitamori, T. Detection of Nonfluorescent Molecules Using Differential Interference Contrast Thermal Lens Microscope for Extended Nanochannel Chromatography. *J. Sep. Sci.* **2011**, *34*, 2920–2924.

Šikovec, M.; Novič, M.; Hudnik, V.; Franko, M. On-Line Thermal Lens Spectrometric Detection of Cr(III) and Cr(VI) after Separation by Ion Chromatography. *J. Chromatogr. A* **1995**, *706*, 121–126.

Šikovec, M.; Novič, M.; Franko, M. Application of Thermal Lens Spectrometric Detection to the Determination of Heavy Metals by Ion Chromatography. *J. Chromatogr. A* **1996**, *739*, 111–117.

Šikovec, M.; Franko, M.; Novič, M.; Veber, M. Effect of Organic Solvents in the On-Line Thermal Lens Spectrometric Detection of Chromium(III) and Chromium(VI) after Ion Chromatographic Separation. *J. Chromatogr. A* **2001**, *920*, 119–125.

Slyadnev, M. N.; Tanaka, Y.; Tokeshi, M.; Kitamori, T. Photothermal Temperature Control of a Chemical Reaction on a Microchip Using an Infrared Diode Laser. *Anal. Chem.* **2001**, *73*, 4037–4044.

Smirnova, A.; Mawatari, K.; Hibara, A.; Proskurnin, M. A.; Kitamori, T. Micro-multiphase Laminar Flows for the Extraction and Detection of Carbaryl Derivative. *Anal. Chim. Acta* **2006**, *558*, 69–74.

Smirnova, A.; Shimura, K.; Hibara, A.; Proskurnin, M. A.; Kitamori, T. Application of a Micro Multiphase Laminar Flow on a Microchip for Extraction and Determination of Derivatized Carbamate Pesticides. *Anal. Sci.* **2007**, *23*, 103–107.

Smirnova, A.; Proskurnin, M. A.; Bendrysheva, S. N.; Nedosekin, D. A.; Hibara, A.; Kitamori, T. Thermooptical Detection in Microchips: From Macro- to Micro-scale with Enhanced Analytical Parameters. *Electrophoresis* **2008**, *29*, 2741–2753.

Smirnova, A.; Proskurnin, M. A.; Mawatari, K.; Kitamori, T. Desktop Near-Field Thermal-Lens Microscope for Thermo-Optical Detection in Microfluidics. *Electrophoresis* **2012**, *33*, 2748–2751.

Sorouraddin, H. M.; Hibara, A.; Proskurnin, M. A.; Kitamori, T. Integrated FIA for the Determination of Ascorbic Acid and Dehydroascorbic Acid in a Microfabricated Glass-Channel by Thermal Lens Microscopy. *Anal. Sci.* **2000**, *16*, 1033–1037.

Sorouraddin, H. M.; Hibara, A.; Kitamori, T. Use of a Thermal Lens Microscope in Integrated Catecholamine Determination on a Microchip. *Fresenius' J. Anal. Chem.* **2001**, *371*, 91–96.

Surmeian, M.; Slyadnev, M. N.; Hisamoto, H.; Hibara, A.; Uchiyama, K.; Kitamori, T. Three-Layer Flow Membrane System on a Microchip for Investigation of Molecular Transport. *Anal. Chem.* **2002**, *74*, 2014–2020.

Takeshita, K.; Shibato, J.; Sameshima, T.; Fukunaga, S.; Isobe, S.; Arihara, K.; Itoh, M. Damage of Yeast Cells Induced by Pulsed Light Irradiation. *Int. J. Food Microbiol.* **2003**, *85*, 151–158.

Tamaki, E.; Sato, K.; Tokeshi, M.; Sato, K.; Aihara, M.; Kitamori, T. Single Cell Analysis by a Scanning Thermal Lens Microscope with a Microchip: Direct Monitoring of Cytochrome-c Distribution during Apoptosis Process. *Anal. Chem.* **2002**, *74*, 1560–1564.

Tamaki, E.; Hibara, A.; Tokeshi, M.; Kitamori, T. Microchannel-Assisted Thermal-Lens Spectrometry for Microchip Analysis. *J. Chromatogr. A* **2003**, *987*, 197–204.

Tamaki, E.; Hibara, A.; Tokeshi, M.; Kitamori, T. Tunable Thermal Lens Spectrometry Utilizing Microchannel-Assisted Thermal Lens Spectrometry. *Lab Chip* **2005**, *5*, 129–131.

Tanaka, Y.; Slyadnev, M. N.; Hibara, A.; Tokeshi, M.; Kitamori, T. Non-contact Photothermal Control of Enzyme Reactions on a Microchip by Using a Compact Diode Laser. *J. Chromatogr. A* **2000**, *894*, 45–51.

Tanaka, Y.; Kikukawa, Y.; Sato, K.; Sugii, Y.; Kitamori, T. Culture and Leukocyte Adhesion Assay of Human Arterial Endothelial Cells in a Glass Microchip. *Anal. Sci.* **2007**, *23*, 261–266.

Taouri, A.; Derbal, H.; Nunzi, J. M.; Mountasser, R.; Sylla, M. Two-Photon Absorption Cross-Section Measurement by Thermal Lens and Nonlinear Transmission Methods in Organic Materials at 532 nm and 1064 nm Laser Excitations. *J. Optoelectron. Adv. M* **2009**, *11*, 1696–1703.

Tian, W.-C.; Finhout, E. *Microfluidics for Biological Applications*; Springer Science+Business Media: New York, 2008.

Tokeshi, M.; Uchida, M.; Uchiyama, K.; Sawada, T.; Kitamori, T. Single- and Countable-Molecule Detection of Non-Fluorescent Molecules in Liquid Phase. *J. Lumin.* **1999**, *83–84*, 261–264.

Tokeshi, M.; Minagawa, T.; Kitamori, T. Integration of a Microextraction System on a Glass Chip: Ion-Pair Solvent Extraction of Fe (II) with 4,7-Diphenyl-1,10- Phenanthrolinedisulfonic Acid and Tri-*n*-octylmethylammonium Chloride. *Anal. Chem.* **2000**, *72*, 1711–1714.

Tokeshi, M.; Sato, K.; Kitamori, T. Integration Chemistry for Biochip: Integration of Immunoassay and Bio-Chemical Lab on a Chip. *RIKEN Rev.* **2001a**, *36*, 24–25.

Tokeshi, M.; Uchida, M.; Hibara, A.; Sawada, T.; Kitamori, T. Determination of Subyoctomole Amounts of Nonfluorescent Molecules Using a Thermal Lens Microscope: Subsingle-Molecule Determination. *Anal. Chem.* **2001b**, *73*, 2112–2116.

Tokeshi, M.; Minagawa, T.; Uchiyama, K.; Hibara, A.; Sato, K.; Hisamoto, H.; Kitamori, T. Continuous Flow Chemical Processing on a Microchip by Combining Micro Unit Operations and a Multiphase Flow Network. *Anal. Chem.* **2002**, *74*, 1565 –1571.

Tokeshi, M.; Kikutani, Y.; Hibara, A.; Sato, K.; Hisamoto, H.; Kitamori, T. Chemical Processing on Microchips for Analysis, Synthesis, and Bioassay. *Electrophoresis* **2003**, *24*, 3583–3594.

Tokeshi, M.; Yamaguchi, J.; Hattori, A.; Kitamori, T. Micro Thermal Lens Optical Systems. *Anal. Chem.* **2005**, *77*, 626–630.

Tran, C. D. Simultaneous Enhancement of Fluorescence and Thermal Lensing by Reversed Micelles. *Anal. Chem.* **1988**, *60*, 182–185.

Tran, C. D.; Grishko, V. I. Thermal Lens Technique for Sensitive and Nondestructive Determination of Isotopic Purity. *Anal. Biochem.* **1994**, *218*, 197–203.

Tran, C. D.; Simianu, V. Multiwavelength Thermal Lens Spectrophotometer Based on an Acousto-optic Tunable Filter. *Anal. Chem.* **1992**, *64*, 1419–1425.

Tran, C. D.; Van Fleet, T. A. Micellar Induced Simultaneous Enhancement of Fluorescence and Thermal Lensing. *Anal. Chem.* **1988**, *60*, 2478–2482.

Tran, C. D.; Zhang, W. Thermal Lensing Detection of Lanthanide Ions by Solvent Extraction Using Crown Ethers. *Anal. Chem.* **1990**, *62*, 830–834.

Tran, C. D.; Grishko, V. I.; Baptista, M. S. Nondestructive and Nonintrusive Determination of Chemical and Isotopic Purity of Solvents by Near-Infrared Thermal Lens Spectrometry. *Appl. Spectrosc.* **1994**, *48*, 833–842.

Tran, C. D.; Challa, S.; Franko, M. Ionic Liquids as an Attractive Alternative Solvent for Thermal Lens Measurements. *Anal. Chem.* **2005**, *77*, 7442–7447.

Uchiyama, K.; Hibara, A.; Sato, K.; Hisamoto, H.; Tokeshi, M.; Kitamori, T. An Interface Chip Connection between Capillary Electrophoresis and Thermal Lens Microscope. *Electrophoresis* **2003**, *24*, 179–184.

Uchiyama, K.; Tokeshi, M.; Kikutani, Y.; Hattori, A.; Kitamori, T. Optimization of an Interface Chip for Coupling Capillary Electrophoresis with Thermal Lens Microscopic Detection. *Anal. Sci.* **2005**, *21*, 49–52.

Váradi, M.; Balla, J.; Pungor, E. Comparison of Electrochemical Detectors with Non-electrochemical Detectors in Chromatography. *Pure Appl. Chem.* **1979**, *51*, 1175–1182.

Voelkel, R.; Weible, K. J. Laser Beam Homogenizing: Limitations and Constraints. In *Optical Fabrication, Testing and Metrology III*; SPIE: Bellingham, WA, 2008.

Vyas, R.; Gupta, R. Photothermal Lensing Spectroscopy in a Flowing Medium: Theory. *Appl. Opt.* **1988**, *27*, 4701–4711.

Weimer, W. A.; Dovichi, N. J. Optimization of Photothermal Refraction for Flowing Liquid Samples. *Appl. Spectrosc.* **1985**, *39*, 1009–1013.

Wu, J.; Gu, M. Microfluidic Sensing: State of the Art Fabrication and Detection Techniques. *J. Biomed. Opt.* **2011**, *16*, 080901.

Xu, M.; Tran, C. D. Thermal Lens-Circular Dichroism Detector for High-Performance Liquid Chromatography. *Anal. Chem.* **1990a**, *62*, 2467–2471.

Xu, M.; Tran, C. D. Thermal Lens-Circular Dichroism Spectropolarimeter. *Appl. Spectrosc.* **1990b**, *44*, 962–966.

Yamasaki, Y.; Goto, M.; Kariyasaki, A.; Morooka, S.; Yamaguchi, Y.; Miyazaki, M.; Maeda, H. Layered Liquid-Liquid Flow in Microchannels Having Selectively Modified Hydrophilic and Hydrophobic Walls. *Korean J. Chem. Eng.* **2009**, *26*, 1759–1765.

Yamauchi, M.; Mawatari, K.; Hibara, A.; Tokeshi, M.; Kitamori, T. Circular Dichroism Thermal Lens Microscope for Sensitive Chiral Analysis on Microchip. *Anal. Chem.* **2006a**, *78*, 2646–2650.

Yamauchi, M.; Tokeshi, M.; Yamaguchi, J.; Fukuzawa, T.; Hattori, A.; Hibara, A.; Kitamori, T. Miniaturized Thermal Lens and Fluorescence Detection System for Microchemical Chips. *J. Chromatogr. A* **2006b**, *1106*, 89–93.

Yu, F.; Kachanov, A. A.; Koulikov, S.; Wainright, A.; Zare, R. N. Ultraviolet Thermal Lensing Detection of Amino Acids. *J. Chromatogr. A* **2009**, *1216*, 3423–3430.

Zhang, J.; Huang, Y.; Chuang, C.-J.; Bivolarska, M.; See, C. W.; Somekh, M. G.; Pitter, M. C. Polarization Modulation Thermal Lens Microscopy for Imaging the Orientation of Non-spherical Nanoparticles. *Opt. Express* **2011**, *19*, 2643–2648.

Zheng, J.; Odake, T.; Kitamori, T.; Sawada, T. Fast Slab Gel Electrophoretic Separation of DNA Fragments with a Short Migration Distance Using Thermal Lens Microscope. *Anal. Sci.* **1999a**, *15*, 223–227.

Zheng, J.; Odake, T.; Kitamori, T.; Sawada, T. Miniaturized Ultrathin Slab Gel Electrophoresis with Thermal Lens Microscope Detection and Its Application to Fast Genetic Diagnosis. *Anal. Chem.* **1999b**, *71*, 5003–5008.

Žnidaršič-Plazl, P.; Plazl, I. Steroid Extraction in a Microchannel SystemMathematical Modeling and Experiments. *Lab Chip* **2007**, *7*, 883–889.